Advances in Continuous and Discrete Models

RESEARCH Open Access

The effect of time delay on the dynamics of a fractional-order epidemic model

Wanqin Wu[1,2], Jianwen Zhou[1*], Zhixiang Li[2*] and Xuewen Tan[2]

*Correspondence:
jwzhou@ynu.edu.cn;
23213037570007@ymu.edu.cn
[1]Department of Mathematics, Yunnan University, Kunming, 650091 Yunnan, P.R. China
[2]Department of Mathematics, Yunnan Minzu University, Kunming, 650500 Yunnan, China

Abstract

This study establishes a novel time-delay fractional SEIHR infectious disease model to investigate the effects of saturated incidence rates and time delays on different populations, including susceptibles, infected individuals, recovered individuals, and latent infected individuals. First, the existence and boundedness of the model's solutions are verified, confirming its well-posedness. Subsequently, the existence of equilibria is analyzed, and the impact of parameter variations on the system is explored by examining the equilibria ϵ_0 and ϵ_*, as well as the basic reproduction number R_0. Additionally, the global dynamics of the equilibria are further analyzed using the Lyapunov method, while Hopf bifurcation theory is applied to explore the conditions under which the system shifts from stability to oscillatory behavior. Numerical simulations further validate the theoretical analysis, showing that time-delay effects significantly influence the system's responsiveness and the rate of disease transmission. Moreover, when the time delay τ crosses the critical threshold τ_0, the system exhibits periodic oscillations. By predicting periodic fluctuations and incorporating memory effects and persistent influences, we can better control epidemics, emphasizing the importance of time-delay adjustments and enhancing the system's biological realism.

Keywords: Time-delay; Fractional; Saturated incidence rates; Global dynamics; Bifurcation theory

1 Introduction

Despite significant advances in healthcare and preventive measures in recent years, infectious diseases remain a leading cause of high mortality in affected communities [1, 2]. This persistence is not only due to the continuous mutation of pathogens but also results from socio-economic challenges, inadequate public health infrastructure, and limited health education. The ongoing threat of infectious diseases places a heavy burden on healthcare systems, drives up medical costs [3], and, in severe cases, can lead to community instability. Therefore, effectively controlling the spread of disease is crucial.

Mathematical modeling plays a key role in both epidemiological and pest–predator ecosystem studies [4, 5], helping researchers identify the driving factors of systems and assess intervention strategies. By simulating disease transmission or ecological dynamics under various conditions, models assist in understanding the interactions between species

and provide a basis for determining control measures [6]. In epidemiology, disease transmission models illustrate the interactions between pathogens and hosts, revealing how interventions (such as vaccination or isolation) can effectively reduce transmission. Similarly, pest–predator models reflect how predators control pest populations [7], demonstrating balance mechanisms within ecosystems. While medical advances in diagnosis and treatment are crucial, mathematical models in epidemiology and ecology remain essential tools for mitigating disease transmission, optimizing control measures, and advancing eradication efforts.

In recent years, infectious disease modeling has become crucial in epidemiology, aiding researchers in understanding transmission patterns and devising effective control strategies. The foundational SIR model, which classifies populations into susceptible, infected, and recovered groups, was first introduced by Bernoulli in 1760 [8] and later expanded by McKendrick and Kermack [9]. To improve model accuracy, additional compartments, such as "exposed" and "hospital isolation" [10–13], have been introduced to capture the effects of latency periods and the role of hospital isolation in disease transmission.

In these models, the incidence rate is a key parameter for measuring new infections. Due to the complexity of disease transmission, various nonlinear incidence models have been developed, including bilinear incidence rates βSI describing the interaction between susceptible and infected individuals [14, 15], fractional incidence rates $\beta S\frac{I}{S+I}$ accounting for memory effects [16], nonmonotonic incidence rates $\frac{\beta SI}{1+kI^2}$ modeling varying infection dynamics [17, 18], and saturated incidence models representing transmission limitations due to factors like healthcare capacity or immunity [4, 19]. The saturated incidence model, introduced by Capasso and Serio [20], is expressed as $g(I) = \frac{\beta I}{1+mI}$, where the suppression term $1 + mI$ in the denominator limits transmission rates at high infection levels. Jan and Bentaleb [6, 21] later enhanced this model by incorporating an infection saturation parameter m, which improves responsiveness under high infection levels and enables further exploration of m's impact on population dynamics.

To better capture latency and immune response delays, time-delay differential equations are commonly used in infectious disease models [22–24]. Delay parameters account for latent infection periods and immune response delays, which are crucial for understanding disease dynamics and optimizing control strategies. For example, Wang and Zhu [25, 26] explored global dynamics with dual delays, while Ilhem and Barman [22, 27, 28] examined the effects of these delays on stability and Hopf bifurcations. Delays also play a key role in evaluating vaccine-induced immunity, especially when natural delays in the viral lifecycle are considered [29, 30], enhancing the biological realism of the model.

The introduction of fractional calculus has further expanded infectious disease modeling. Fractional calculus describes derivatives of arbitrary orders, incorporating memory effects and nonlocal influences [31]. When combined with time-delay mechanisms, fractional calculus allows for a better representation of complex immune delays and viral mutations [22, 32]. Compared to integer-order systems, fractional-order systems provide a broader range of stability properties, with applications in epidemiology, physics, and other scientific fields [33–35]. The Caputo definition is widely used in biological modeling due to its compatibility with standard initial condition settings [36, 37].

Currently, many studies have developed infectious disease models to analyze dynamic interactions between population groups [10, 13], often assuming a fixed transmission rate [4, 15] without accounting for how population density affects transmission variability. To

address this, our study incorporates a saturated incidence rate model to better simulate transmission changes. Existing models also have room for improvement in capturing complex compartment interactions and immune response delays [24, 27, 28].

To this end, we propose a new time-delay fractional-order SEIHR model, which includes traditional compartments (susceptible, exposed, infectious, and recovered) along with a hospital isolation compartment. The fractional-order aspect adds biological realism by incorporating memory effects, capturing how past infections and immune responses influence current dynamics. This model thus provides a more accurate depiction of disease transmission, incorporating immune delays and nonlinear incidence rates for a more comprehensive analysis of epidemic dynamics.

The key contributions and innovations of this paper are outlined as follows:

a. Unlike previous studies [10, 22], this study presents a novel time-delay fractional SEIHR model that combines fractional differential equations with time delays to more accurately simulate infectious disease transmission. By incorporating memory effects and persistent influences among population groups, as shown in Fig. 2 and Fig. 3, this approach enhances the system's biological realism.
b. The system incorporates a saturated incidence rate to reflect dynamic changes in transmission at high infection levels. This nonlinear structure realistically depicts transmission limitations in densely populated settings, thereby improving the accuracy of epidemic trend predictions.
c. Using the Lyapunov method and Hopf bifurcation theory, this study provides an in-depth analysis of the global dynamics and bifurcation behavior at equilibrium points, revealing the conditions under which the system transitions from stability to oscillatory behavior. This analysis offers new insights into the dynamic mechanisms of infectious disease spread, as illustrated in Figs. 10–17.

The structure of the remainder of this paper is as follows: The second section provides relevant preparatory knowledge. The third section presents the development of the new system. The fourth section conducts a dynamic analysis of the system. The fifth section performs numerical simulations to validate the theoretical results presented in the previous section. Finally, the paper concludes with a summary of the research and an overview of future directions.

2 Model formulation and preliminaries

2.1 Model formulation

Building on previous research, this study introduces a system that integrates saturated incidence rates, time-delay effects, and hospitalization dynamics to investigate epidemic transmission under varying conditions of heterogeneity. The following new system is

given:

$$\begin{cases} \dfrac{dS}{dt} = \Pi - g(I)S(t) - \mu S(t) + \xi R(t), \\ \dfrac{dE}{dt} = g(I(t))S(t) - \mu E(t) - \delta E(t), \\ \dfrac{dI}{dt} = \delta E(t) - (\mu + \mu_1 + r_1 + \eta)I(t), \\ \dfrac{dH}{dt} = \eta I(t) - (\mu + \mu_2 + r_2)H(t), \\ \dfrac{dR}{dt} = r_1 I(t) + r_2 H(t) - (\mu + \xi)R(t). \end{cases} \tag{1}$$

Incorporating the Caputo fractional derivative of noninteger order, which more effectively captures the memory effects and nonlocal characteristics of the system, we extend the model to include time delays and saturated incidence rates $g(I) = \frac{bI}{1+mI}$. The resulting sys-

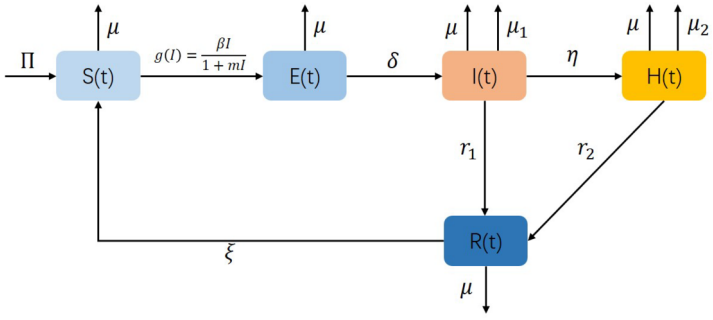

Figure 1 Flowchart of infectious disease transmission under the effect of time delay

Table 1 Definitions of parameters for system (2)

Parameters	Profile	Unit
Π	Recruitment rate	day^{-1}
β	The transmission rate of the infection	day^{-1}
μ	The level of mortality affecting the population	day^{-1}
δ	The transition rate of the exposed population	day^{-1}
μ_1	Mortality rate of infected individuals due to the disease	day^{-1}
μ_2	Mortality rate of hospitalized isolated individuals due to the disease	day^{-1}
r_1	The recovery rate of individuals in the infected compartment	day^{-1}
r_2	The recovery rate of hospitalized isolated individuals	day^{-1}
η	Isolation rate of infected individuals transitioning to hospitalization	day^{-1}
ξ	The speed at which individuals transition from the recovered group back into the susceptible group	day^{-1}
m	Suppression factor or infection saturation parameter	$person^{-1}$
S	Susceptible population	*persons*
E	Exposed individuals	*persons*
I	Infected individuals	*persons*
H	Hospitalized population	*persons*
R	Recovered individuals	*persons*

tem is represented by the following fractional-order equations:

$$\begin{cases} {}_0^C D_t^\alpha S(t) = \Pi - \mu S(t) - \dfrac{\beta S(t) I(t)}{1 + mI(t)} + \xi R(t), \\ {}_0^C D_t^\alpha E(t) = \dfrac{\beta S(t) I(t)}{1 + mI(t)} - \mu E(t) - \delta E(t-\tau), \\ {}_0^C D_t^\alpha I(t) = \delta E(t-\tau) - (\mu + \mu_1 + r_1 + \eta) I(t), \\ {}_0^C D_t^\alpha H(t) = \eta I(t) - (\mu + \mu_2 + r_2) H(t), \\ {}_0^C D_t^\alpha R(t) = r_1 I(t) + r_2 H(t) - (\mu + \xi) R(t). \end{cases} \tag{2}$$

The basic transmission process is illustrated in Fig. 1, and the biological significance of each parameter is summarized in Table 1. The initial conditions are specified as follows:

$$S(t_0) = S_0, E(t_0) = E_0, I(t_0) = I_0, H(t_0) = H_0, R(t_0) = R_0. \tag{3}$$

2.2 Preliminaries

Definition 2.1 ([34]) The Caputo fractional derivative of order $\eta > 0$ for a function $f : C^n[t_0, \infty) \to \mathbb{R}$ is given by

$$D^\eta f(t) = \frac{1}{\Gamma(n-\eta)} \int_{t_0}^t \frac{f^{(n)}(\tau)}{(t-\tau)^{\eta-n+1}} d\tau,$$

where $C^n[t_0, \infty)$ denotes the space of functions that are n times continuously differentiable on $[t_0, \infty)$, $\Gamma(n)$ is the gamma function, n is a positive integer satisfying $n - 1 < \eta < n$, and $t > t_0$. Specifically, when $0 < \eta < 1$, the definition simplifies to

$$D^\eta f(t) = \frac{1}{\Gamma(1-\eta)} \int_{t_0}^t \frac{f'(\tau)}{(t-\tau)^\eta} d\tau.$$

Lemma 2.1 ([38]) *Let $g(t) \in \mathbb{R}_+$ be a continuous and differentiable function, then*

$$D_t^\theta \left[g(t) - g^* - g^* \ln \frac{g(t)}{g^*} \right] \le \left(1 - \frac{g^*}{g(t)} \right) D_t^\theta g(t),$$

where $g^* \in \mathbb{R}_+$, $\forall \theta \in (0, 1]$.

Lemma 2.2 ([39]) *Assume $f \in C[a, b]$ and $D^\theta f \in C[a, b]$ for $0 < \theta \le 1$. Then there exists a point $\xi(x) \in [a, x]$ such that*

$$f(x) = f(a) + \frac{1}{\theta} D^\theta f(\xi)(x-a)^\theta.$$

Lemma 2.3 ([37]) *Let $\theta \in (0, 1)$ and suppose $G : [t_0, \infty) \to \mathbb{R}$ is a continuous function that satisfies the condition below*

$$D^\theta G(t) + \mu G(t) \le \nu, \quad t \ge t_0, \quad \mu, \nu \in \mathbb{R}, \quad \mu \ne 0.$$

Then the following inequality holds:

$$G(t) \leq \left(G(t_0) - \frac{\nu}{\mu} \right) E_\theta \left(-\mu (t - t_0)^\theta \right) + \frac{\nu}{\mu}$$

for all $t \geq t_0$, *where* E_θ *is the Mittag-Leffler function of one parameter defined by*

$$E_\theta(t) = \sum_{k=0}^{\infty} \frac{t^k}{\Gamma(\theta k + 1)}.$$

Lemma 2.4 ([40]) *Suppose that* $x^* \in \Upsilon \subset \mathbb{R}^n$ *is an equilibrium for system*

$$D^\theta x(t) = f(t, x(t)), \quad t \geq t_0,$$

and consider a continuously differentiable function $V(t,x) : [t_0, \infty) \times \Upsilon \to \mathbb{R}$ *that fulfills the following conditions*:

$$Q_1(x) \leq V(t,x) \leq Q_2(x),$$
$$D^\alpha V(t,x) \leq -Q_3(x),$$

for $t \geq t_0$ *and* $x \in \Upsilon$, *where* $Q_i(x)$, $i = 1, 2, 3$, *are continuous and positive-definite functions on* Υ. *Under these conditions,* x^* *is uniformly asymptotically stable*.

Lemma 2.5 ([41]) *Let* $\alpha \in (0, 1]$, $\Omega \subset \mathbb{R}^n$ *be a domain, and let* $F : [t_0, \infty) \times \Omega \to \mathbb{R}^n$ *be a function satisfying the Lipschitz condition with respect to* ξ. *Consider the following fractional-order differential equation*:

$$D^\alpha \xi(t) = F(t, \xi(t)), \quad t > t_0,$$

subject to the initial condition $\xi(t_0) = \xi_0 \in \Omega$. *Under these conditions, the system has a unique maximal solution.*

3 The dynamical analysis of system (2)

3.1 Existence and uniqueness of solutions

We will rely on the following lemma as the basis for the proof.

Lemma 3.1 *Consider the fractional-order system given by*

$${}_0^C D_t^\alpha u(t) = h(t, u), \quad u(t_0) = u_0,$$

where $\alpha \in (0, 1]$ *and* $t_0 > 0$. *Let* $h : [t_0, \infty) \times \Omega \to \mathbb{R}^n$ *satisfy the following Lipschitz condition* [41] *with respect to* u:

$$|h(t, u_1) - h(t, u_2)| \leq L|u_1 - u_2|, \quad \forall u_1, u_2 \in \Omega, \forall t \geq t_0,$$

for some constant $L > 0$. *Under these conditions, system* (2) *admits a unique solution* $u(t)$ *over the interval* $[t_0, \infty) \times \Omega$.

Theorem 3.1 *For any initial point* $\Xi_{t_0} = \left(S_{t_0}, E_{t_0}, I_{t_0}, H_{t_0}, R_{t_0}\right) \in \Sigma$ *within system* (2), *there exists a unique solution* $\Xi_t = (S(t), E(t), I(t), H(t), R(t)) \in \Sigma$ *for all* $t > t_0$.

Proof First, consider the interval $\Sigma \times [t_0, t_1]$, where

$$\Sigma = \{(S, E, I, H, R) \in \mathbb{R}^5 : \max\{|S|, |E|, |I|, |H|, |R|\} \leq K\}.$$

In this region, all variables are constrained to not exceed the upper bound K. Here, t_1 and K are finite positive constants. Let $U_1 = (S, E, I, H, R)$ and $U_2 = (S_1, E_1, I_1, H_1, R_1)$ be two points within Σ, and define a mapping $M : \Sigma \to \mathbb{R}^5$ such that $M(\Xi) = (M_1(\Xi), M_2(\Xi), M_3(\Xi), M_4(\Xi), M_5(\Xi))$, where

$$\begin{aligned}
M_1(\Xi) &= \Pi - \mu S(t) - \frac{\beta S(t) I(t)}{1 + mI(t)} + \xi R(t), \\
M_2(\Xi) &= \frac{\beta S(t) I(t)}{1 + mI(t)} - \mu E(t) - \delta E(t - \tau), \\
M_3(\Xi) &= \delta E(t - \tau) - (\mu + \mu_1 + r_1 + \eta) I(t), \\
M_4(\Xi) &= \eta I(t) - (\mu + \mu_2 + r_2) H(t), \\
M_5(\Xi) &= r_1 I(t) + r_2 H(t) - (\mu + \xi) R(t).
\end{aligned}$$

For any $U_1, U_2 \in \Sigma$, the following inequality holds:

$$\|M(U_1) - M(U_2)\| \leq N \|U_1 - U_2\|, \tag{4}$$

where

$$\begin{aligned}
M_1(U_1) - M_1(U_2) &= \left| -\mu(S - S_1) - \beta \left(\frac{SI}{1 + mI} - \frac{S_1 I_1}{1 + mI_1} \right) + \xi(R - R_1) \right|, \\
M_2(U_1) - M_2(U_2) &= \left| \beta \left(\frac{SI}{1 + mI} - \frac{S_1 I_1}{1 + mI_1} \right) - \delta \left(E(t - \tau) - E_1(t - \tau) \right) - \mu(E - E_1) \right|, \\
M_3(U_1) - M_3(U_2) &= \left| \delta \left(E(t - \tau) - E_1(t - \tau) \right) - (\mu + \mu_1 + r_1 + \eta)(I - I_1) \right|, \\
M_4(U_1) - M_4(U_2) &= \left| \eta(I - I_1) - (\mu + \mu_2 + r_2)(H - H_1) \right|, \\
M_5(U_1) - M_5(U_2) &= \left| r_1(I - I_1) + r_2(H - H_1) - (\mu + \xi)(R - R_1) \right|.
\end{aligned}$$

We can bound the differences as follows:

$$\begin{aligned}
\|M(U_1) - M(U_2)\| \leq{}& \mu \|S - S_1\| + 2\beta \left| \frac{SI}{1 + mI} - \frac{S_1 I_1}{1 + mI_1} \right| + 2\delta \|E(t - \tau) - E_1(t - \tau)\| \\
&+ \mu \|E - E_1\| + (\mu + \mu_1 + 2r_1 + 2\eta) \|I - I_1\| \\
&+ (\mu + \mu_2 + 2r_2) \|H - H_1\| + (\mu + 2\xi) \|R - R_1\|.
\end{aligned}$$

This simplifies to

$$\|M(U_1) - M(U_2)\| \leq (\mu + 2\beta K) \|S - S_1\| + (2\delta K + \mu) \|E - E_1\|$$

$$+ (\mu + \mu_1 + 2r_1 + 2\eta)\|I - I_1\|$$
$$+ (\mu + \mu_2 + 2r_2)\|H - H_1\| + (\mu + 2\xi)\|R - R_1\|.$$

Finally, we define

$$N_1 = \mu + 2\beta K, \qquad N_2 = 2\delta K + \mu, \qquad N_3 = \mu + \mu_1 + 2r_1 + 2\eta,$$
$$N_4 = \mu + \mu_2 + 2r_2, \qquad N_5 = \mu + 2\xi,$$

and consequently, the inequality can be expressed as

$$\|M(U_1) - M(U_2)\| \leq N_1\|S - S_1\| + N_2\|E - E_1\| + N_3\|I - I_1\| + N_4\|H - H_1\| + N_5\|R - R_1\|.$$

This leads to the validity of equation (4), where $N = \max\{N_1, N_2, N_3, N_4, N_5\}$.

Therefore, M satisfies the Lipschitz condition with respect to $\Xi_t = (S_t, E_t, I_t, H_t, R_t) \in \Sigma$. Thus, by Lemma 2.5, it ensures the existence of a unique solution Ξ_t for system (2) with the initial condition $\Xi_{t_0} = (S_{t_0}, E_{t_0}, I_{t_0}, H_{t_0}, R_{t_0}) \in \Sigma$. □

3.2 Nonnegativity and boundedness of solutions

Positivity and boundedness are crucial for ensuring that the variables in a biological mathematical model stay within realistic and biologically meaningful limits, thereby enhancing the model's biological validity and predictive reliability. Therefore, the solution to system (2) must satisfy these conditions to guarantee the system's accuracy and practical applicability.

Theorem 3.2 *Given the initial state in* (3), *the fractional-order system* (2) *admits a unique solution. Moreover, all solutions of systems* (1)–(2) *are positive, bounded, and asymptotically converge to a compact attractor.*

Proof As known from Theorem 4.1, for any t, a singular solution exists, given the initial state Ξ_{t_0}. To prove that $S \geq 0$, we use a proof by contradiction. Suppose that there exists a time $t_1 > t_0$ (or $t_1 > 0$) such that $S(t) > 0$ for all $t \in [0, t_1)$, but $S(t) < 0$ for $t \in (t_1, t_1 + \varepsilon_1]$ with $S(t_1) = 0$, where $\varepsilon_1 > 0$ is sufficiently small. Examining the first equation of system (2), we can obtain

$$D_t^\theta S(t)\Big|_{t=t_1} = \Pi > 0.$$

Thus, by Lemma 2.2, there exists a value $\xi_1 \in (t_1, t_1 + \varepsilon_1]$ such that

$$S(t_1 + \varepsilon_1) = S(t_1) + \frac{1}{\alpha} D_t^\alpha S(\xi_1)\varepsilon_1^\alpha.$$

By choosing ε_1 to be sufficiently small, it follows that $S(t_1 + \varepsilon_1) > 0$, which contradicts the assumption that $S(t) < 0$ for $t \in (t_1, t_1 + \varepsilon_1]$. Therefore, we conclude that $S(t) \geq 0$ for all $t \geq 0$.

To prove that $E \geq 0$, we use a proof by contradiction. Suppose that there exists a time $t_2 > 0$ such that $E(t) > 0$ for all $t \in [0, t_2)$, but $E(t) < 0$ for $t \in (t_2, t_2 + \varepsilon_2]$ with $E(t_2) = 0$, where

$\varepsilon_2 > 0$ is sufficiently small. Examining the second equation of system (2), we can obtain

$$D_t^\theta E(t)\Big|_{t=t_2} = \frac{\beta S(t)I(t)}{1 + mI(t)} \geq 0.$$

According to Lemma 2.2, we obtain a value $\xi_2 \in (t_2, t_2 + \varepsilon_2]$ such that

$$E(t_2 + \varepsilon_2) = E(t_2) + \frac{1}{\theta} D_t^\theta E(\xi_2)\varepsilon_2^\theta.$$

By selecting ε_2 to be sufficiently small, it follows that $E(t_2 + \varepsilon_2) > 0$, which contradicts the assumption that $E(t) \leq 0$ for $t \in [t_2, t_2 + \varepsilon_2]$. Therefore, we conclude that $E(t) \geq 0$ for all $t \geq 0$.

Building upon the previous discussion regarding the groups S and E in system (2) and utilizing the same theoretical framework, it can be demonstrated that $I \geq 0$, $H \geq 0$, and $R \geq 0$ also hold true.

Now, we proceed to establish the boundedness of system (2). To this end, let us define the following quantity:

$$T(t) = S(t) + E(t) + I(t) + H(t) + R(t).$$

The fractional derivative of the above expression is

$$\begin{aligned} D_t^\alpha T(t) &= D_t^\alpha S(t) + D_t^\alpha E(t) + D_t^\alpha I(t) + D_t^\alpha H(t) + D_t^\alpha R(t) \\ &= \Pi - \mu S - \mu E - (\mu + \mu_1)I - (\mu + \mu_2)H - \mu R \\ &= \Pi - \mu(S + E + I + H + R) - (\mu_1 I + \mu_2 H) \\ &\leq \Pi - \mu T(t), \end{aligned}$$

yielding $D_t^\alpha T(t) \leq \Pi - \mu T(t)$. By Lemma 2.3, it follows that

$$T(t) \leq \frac{\Pi}{\mu} + (T_{t_0}(t) - \frac{\Pi}{\mu})E_\alpha(-\mu(t - t_0)^\alpha),$$

where $T_{t_0}(t) = S_{t_0}(t) + E_{t_0}(t) + I_{t_0}(t) + H_{t_0}(t) + R_{t_0}(t)$, ensuring the existence of a limit

$$\lim_{x \to +\infty} sup T(t) \leq \frac{\Pi}{\mu}.$$

Consequently, the solutions of system (2) are reliably bounded, and the positive attractor set for system (2) is given by

$$\Theta = \left\{ (S, E, I, H, R) \in \mathbb{R}_+^5 : 0 < S + E + I + H + R \leq \frac{\Pi}{\delta} \right\}. \tag{5}$$

Thus, Theorem 4.2 is proven. □

3.3 Existence of equilibria

System (2) has two equilibria: one corresponding to the absence of disease and the other representing a state of endemic disease persistence. To determine the equilibria where the system's variables are constant, the derivatives of all state variables must equal zero. This ensures that each variable is in a steady state, satisfying the conditions for equilibrium. We examine the conditions under which the right-hand side of system (2) equals zero, leading to the system's equilibria. This yields the following set of equations:

$$\begin{cases} \Pi - \frac{\beta S(t)I(t)}{1+mI(t)} - \mu S(t) + \xi R(t) = 0, \\ \frac{\beta S(t)I(t)}{1+mI(t)} - \mu E(t) - \delta E(t-\tau) = 0, \\ \delta E(t-\tau) - (\mu + \mu_1 + r_1 + \eta)I(t) = 0, \\ \eta I(t) - (\mu + \mu_2 + r_2)H(t) = 0, \\ r_1 I(t) + r_2 H(t) - (\mu + \xi)R(t) = 0. \end{cases} \tag{6}$$

System (2) consistently admits a disease-free equilibrium, denoted by $\epsilon_0 = \left(\frac{\Pi}{\mu}, 0, 0, 0, 0\right)$. When $\epsilon_* = I = H = R = 0$, this equilibrium fulfills the following equation:

$$\Pi - \mu S(t) + \xi R(t) - \frac{\beta S(t)I(t)}{1 + mI(t)} = 0.$$

When E, I, H, and R are all nonzero, and $R_0 > 1$, the system features an endemic equilibrium, symbolized by $\epsilon_* = (S^*, E^*, I^*, H^*, R^*)$. This equilibrium satisfies the following set of equations:

$$\Pi = \mu S^* + \frac{\beta S^* I^*}{1 + mI^*} - \xi R^*, \quad \frac{\beta S^* I^*}{1 + mI^*} = \mu E^* + \delta E^*(t-\tau),$$
$$(\mu + \mu_1 + r_1 + \eta)I^* = \delta E^*(t-\tau), \quad \eta I^* = (\mu + \mu_2 + r_2)H^*, \quad r_1 I^* + r_2 H^* = (\mu + \xi)R^*.$$

The equilibria expressions are subsequently obtained as

$$S^* = \frac{\Pi(\mu + \mu_2 + r_2)(\mu + \xi) + \xi I^* (r_1(\mu + \mu_2 + r_2) + r_2\eta)}{(\mu + \mu_2 + r_2)(\mu + \xi)\left(\mu + \frac{\beta I^*}{1+mI^*}\right)},$$
$$E^* = \frac{(\mu + \mu_1 + r_1 + \eta)I^*}{\delta},$$
$$H^* = \frac{\eta I^*}{\mu + \mu_2 + r_2}, \qquad R^* = \frac{r_1 I^*(\mu + \mu_2 + r_2) + r_2\eta I^*}{(\mu + \xi)(\mu + \mu_2 + r_2)}.$$

The value of I^* is determined by solving the following cubic equation:

$$AI^3 + BI^2 + CI + D = 0,$$

where

$$A = \frac{\beta\xi r_1 r_2 \eta m}{(\mu + \mu_2 + r_2)(\mu + \xi)},$$

$$B = \frac{\beta\left(\xi r_1(\mu+\mu_2+r_2)+\xi r_2\eta\right)+(\mu+\delta)(\mu+\mu_1+r_1+\eta)m}{(\mu+\mu_2+r_2)(\mu+\xi)},$$

$$C = \frac{\beta\Pi(\mu+\mu_2+r_2)(\mu+\xi)+(\mu+\delta)(\mu+\mu_1+r_1+\eta)}{(\mu+\mu_2+r_2)(\mu+\xi)},$$

$$D = -\Pi.$$

3.4 Basic reproductive rate(R_0)

The basic reproduction number R_0 is a key parameter that indicates whether an infection will propagate or diminish in a population. Specifically, if $R_0 > 1$, the infection will likely spread, whereas if $R_0 < 1$, it will typically decrease. R_0 is computed using the next-generation matrix [42] approach, given by $\mathcal{H}\mathcal{V}^{-1}$, as

$$R_0 = \rho(\mathcal{H}\mathcal{V}^{-1}), \tag{7}$$

where ρ represents the spectral radius of the matrix $\mathcal{H}\mathcal{V}^{-1}$.

Here, $\mathcal{H}$ is a nonnegative matrix representing new infections caused by infected individuals, and $\mathcal{V}$ is the transfer matrix that describes transitions between individual states. The next-generation matrix $\mathcal{H}\mathcal{V}^{-1}$ provides a means to compute R_0, which serves as a critical threshold for assessing disease transmission dynamics.

From the previous section's proof regarding the existence of equilibria, we identify the disease-free equilibrium as $\epsilon_0 = \left(\frac{\Pi}{\mu}, 0, 0, 0, 0\right)$. Thus, we have

$$H(X) = \begin{pmatrix} g(I)S(t) \\ 0 \\ 0 \end{pmatrix}$$

and

$$V(X) = \begin{pmatrix} \mu E(t) - \delta E(t-\tau) \\ (r_1+\mu_1+\eta+\mu)I(t) - \delta E(t-\tau) \\ (\mu+\mu_2+r_2) - \eta H(t)I(t) \end{pmatrix}.$$

Next, we evaluate the matrices at the disease-free equilibrium

$$\mathcal{H}_{S=\frac{\Pi}{\mu}} = \begin{pmatrix} 0 & \frac{\Pi}{\mu}g'(0) & 0 \\ 0 & 0 & 0 \\ 0 & 0 & 0 \end{pmatrix}$$

and

$$\mathcal{V}_{S=\frac{\Pi}{\mu}} = \begin{pmatrix} \mu+\delta & 0 & 0 \\ -\delta & \mu+\mu_1+r_1+\eta & 0 \\ 0 & -\eta & \mu+\mu_2+r_2 \end{pmatrix}.$$

We can now compute the next-generation matrix

$$\mathcal{H}\mathcal{V}^{-1} = \begin{pmatrix} \frac{\Pi\delta g'(0)}{\mu(\mu+\delta)(\eta+\mu+\mu_1+r_1)} & \frac{\Pi g'(0)}{\mu(\eta+\mu+\mu_1+r_1)} & 0 \\ 0 & 0 & 0 \\ 0 & 0 & 0 \end{pmatrix}.$$

Based on expression (7) and $g(I) = \frac{\beta I}{1+mI}$, we can calculate

$$R_0 = \frac{\beta \Pi \delta}{\mu(\mu+\delta)(\eta+\mu+\mu_1+r_1)}. \tag{8}$$

3.5 Local and global asymptotic stability of equilibria

When $\tau = 0$, the basic reproduction number R_0, the disease-free equilibrium, and the endemic equilibrium of system (2) remain unchanged. In this subsection, we demonstrate that when $\tau \geq 0$, the disease-free equilibrium ϵ_0 is both locally asymptotically stable and globally asymptotically stable. Additionally, when $\tau = 0$, we prove the global asymptotic stability of the endemic equilibrium ϵ_*.

Theorem 3.3 *If $R_0 < 1$, the disease-free equilibrium ϵ_0 of system (2) is locally asymptotically stable for all values of τ. In contrast, if $R_0 > 1$, ϵ_0 becomes unstable for any value of τ.*

Proof The Jacobian matrix of system (2) at the equilibrium ϵ_0 is

$$J_{E_0} = \begin{bmatrix} -\mu & 0 & -\frac{\beta\Pi}{\mu} & 0 & \xi \\ 0 & -\mu-\delta e^{-\lambda\tau} & \frac{\beta\Pi}{\mu} & 0 & 0 \\ 0 & \delta e^{-\lambda\tau} & -(\mu+\mu_1+r_1+\eta) & 0 & 0 \\ 0 & 0 & \eta & -(\mu+\mu_2+r_2) & 0 \\ 0 & 0 & r_1 & r_2 & -(\mu+\xi) \end{bmatrix}.$$

Based on the equation $\det(J - \lambda I) = 0$, the characteristic equation that corresponds is $\Phi_1 \times \Phi_2 = 0$, where

$$\Phi_1 = (\mu+\lambda)(\mu+\xi+\lambda)(\mu+\mu_2+r_2+\lambda)(\mu+\mu_1+r_1+\eta+\lambda),$$

$$\Phi_2 = \left[(\mu+\delta e^{-\lambda\tau}+\lambda) - \frac{\beta\Pi}{\mu(\mu+\mu_1+r_1+\eta+\lambda)} \cdot \delta e^{-\lambda\tau}\right].$$

It is evident that system (2) at equilibrium E_0 always has four negative real roots: $\lambda_{01} = -\mu$, $\lambda_{02} = -\mu-\xi$, $\lambda_{03} = -\mu-\mu_2-r_2$, $\lambda_{04} = -\mu-\mu_1-r_1-\eta$, the remaining eigenvalues satisfy the equation

$$\lambda + \mu + \delta e^{-\lambda\tau} - (\mu+\delta)R_0 \cdot e^{-\lambda\tau} = 0. \tag{9}$$

When $\tau = 0$, we have $\lambda_0 = (\mu+\delta)(R_0-1)$. If $R_0 < 1$, then $\lambda_0 < 0$. Based on the Routh–Hurwitz stability criterion [43, 44], it can be concluded that the disease-free equilibrium ϵ_0 of system (2) exhibits local asymptotic stability.

When $\tau \neq 0$, according to equation (9), we have

$$\lambda = [(\mu+\delta)R_0 - \delta]e^{-\lambda\tau} - \mu,$$

$$Re(\lambda) = e^{-Re(\lambda)}[(\mu+\delta)R_0 - \delta]cos(\tau Im\lambda) - \mu.$$

Assume $Re(\lambda) \geq 0$, then

$$Re(\lambda) \leq (\mu+\delta)R_0 - (\delta+\mu) \leq (\mu+\delta)(R_0-1).$$

Given that $R_0 < 1$, it follows that $\mathrm{Re}(\lambda) < 0$. Consequently, the equilibrium ϵ_0 of system (2) is locally asymptotically stable.

Additionally, for $R_0 > 1$, define $g(\lambda) = \lambda + \mu + \delta e^{-\lambda\tau} - (\mu + \delta)R_0 \cdot e^{-\lambda\tau}$. Since $g(0) < 0$ and $g(+\infty) > 0$, it follows that there exists at least one real positive root. Therefore, the disease-free equilibrium ϵ_0 of system (2) is unsteady.

To summarize the analysis, Theorem 4.3 is proven. □

Theorem 3.4 *If $R_0 \leq 1$, the disease-free equilibrium $\epsilon_0 = \left(\frac{\Pi}{\mu}, 0, 0, 0, 0\right)$ of system (2) is globally asymptotically stable for all $\tau \geq 0$.*

Proof Consider $S(t)$, $E(t)$, $I(t)$, $H(t)$, $R(t)$ as any effective solution to system (2), given the initial condition in (3). Therefore, we construct a Lyapunov function

$$V_0 = \frac{1}{2}(S - S_0)^2 + \theta_1 E + \theta_2 I + \theta_3 H + \theta_4 R + \theta_5 \int_{t-\tau}^{t} E(s)ds. \tag{10}$$

It is evident that V_0 is strictly positive for all variables when they are greater than zero. Thus,

$$D_t^\alpha V_0 \leq (S - S_0)D_t^\alpha S + \theta_1 D_t^\alpha E + \theta_2 D_t^\alpha I + \theta_3 D_t^\alpha H + \theta_4 D_t^\alpha R.$$

Substituting the equations from system (2) into the expression above and setting $f(I) = 1 + mI$ for simplicity, the equation reduces to

$$\begin{aligned}
D_t^\alpha V_0 \leq{}& (S - S_0)\left(\Pi - \mu S - \frac{\beta SI}{f(I)} + \xi R(t)\right) + \theta_1\left(\frac{\beta SI}{f(I)} - \mu E - \delta E(t-\tau)\right) \\
&+ \theta_2\left(\delta E(t-\tau) - (\mu + \mu_1 + r_1 + \eta)I\right) + \theta_3\left(\eta I - (\mu + \mu_2 + r_2)H\right) \\
&+ \theta_4\left(r_1 I + r_2 H - (\mu + \xi)R\right) \\
={}& -\mu(S - S_0)^2 - (S - S_0)\frac{\beta SI}{f(I)} + \xi(S - S_0)R + \frac{\theta_1 \beta SI}{f(I)} \\
&- (\theta_1\mu - \theta_5)E - (\theta_1\delta - \theta_2\delta + \theta_5)E(t-\tau) - [\theta_2(\mu + \mu_1 + r_1 + \eta) - \theta_3\eta - \theta_4 r_1]I \\
&- [\theta_3(\mu + \mu_2 + r_2) - \theta_4 r_4]H - \theta_4(\mu + \xi)R.
\end{aligned}$$

The following conditions are satisfied:

$$\frac{\beta SI}{f(I)} = \frac{\beta I}{f(I)}(S - S_0) + \frac{\Pi\beta I}{\mu f(I)}, \xi(S - S_0)R \leq 0, S_0 = \theta_1 = \frac{\Pi}{\mu}, \theta_1\Pi - (S - S_0)^2 < 0, \tag{11}$$

hence

$$\begin{aligned}
D_t^\alpha V_0 \leq{}& -\mu(S - S_0)^2 - (S - S_0)\frac{\beta I}{f(I)} + \frac{\theta_1\beta\Pi I}{\mu f(I)} + \xi(S - S_0)R \\
&- (\theta_1\mu - \theta_5)E - (\theta_1\delta - \theta_2\delta + \theta_5)E(t-\tau) - [\theta_2(\mu + \mu_1 + r_1 + \eta) - \theta_3\eta - \theta_4 r_1]I \\
&- [\theta_3(\mu + \mu_2 + r_2) - \theta_4 r_2]H - \theta_4(\mu + \xi)R \\
={}& -\mu(S - S_0)^2 - (S - S_0)\frac{\beta I}{f(I)} + \frac{\theta_1\beta\Pi I}{f(I)(\mu + \delta)} + \frac{\theta_1\beta\Pi I\delta}{\mu f(I)(\mu + \delta)} + \xi(S - S_0)R
\end{aligned}$$

$$
\begin{aligned}
&- (\theta_1\mu - \theta_5)E - (\theta_1\delta - \theta_2\delta + \theta_5)E(t-\tau) - [\theta_2(\mu + \mu_1 + r_1 + \eta) - \theta_3\eta - \theta_4 r_1]\, I \\
&- [\theta_3(\mu + \mu_2 + r_2) - \theta_4 r_2]\, H - \theta_4(\mu + \xi)R \\
&= -\mu(S - S_0)^2 + \frac{[\theta_1\Pi - (S - S_0)^2]\beta I}{f(I)(\mu + \delta)} + \frac{\theta_1\beta\Pi I\delta}{\mu f(I)(\mu + \delta)} + \xi(S - S_0)R \\
&- (\theta_1\mu - \theta_5)E - (\theta_1\delta - \theta_2\delta + \theta_5)E(t-\tau) - [\theta_2(\mu + \mu_1 + r_1 + \eta) - \theta_3\eta - \theta_4 r_1]\, I \\
&- [\theta_3(\mu + \mu_2 + r_2) - \theta_4 r_2]\, H - \theta_4(\mu + \xi)R.
\end{aligned}
$$

Case 1: When $R_0 < 1$, we set $\theta_1 = \theta_2$, and since $f(I) = f(0) + f'(0)I + o(I)$, we obtain

$$
\begin{aligned}
&\frac{\theta_1\beta\Pi I\delta}{\mu f(I)(\mu + \delta)} - [\theta_2(\mu + \mu_1 + r_1 + \eta) - \theta_3\eta - \theta_4 r_1]\, I \\
&= \left[\frac{\theta_1\beta\Pi\delta - \mu f(I)(\mu + \delta)(\theta_2(\mu + \mu_1 + r_1 + \eta) - \theta_3\eta - \theta_4 r_1)}{\mu f(I)(\mu + \delta)}\right].
\end{aligned}
$$

For the expression

$$
\begin{aligned}
&\theta_1\beta\Pi\delta - \mu f(I)(\mu + \delta)(\theta_2(\mu + \mu_1 + r_1 + \eta) - \theta_3\eta - \theta_4 r_1) \\
&= \theta_1\beta\Pi\delta - f(0)\mu(\mu + \delta)(\theta_2(\mu + \mu_1 + r_1 + \eta) - \theta_3\eta - \theta_4 r_1) \\
&- \mu(\mu + \delta)(\theta_2(\mu + \mu_1 + r_1 + \eta) - \theta_3\eta - \theta_4 r_1)(f'(0)I + o(I)) \\
&\le -\theta_1\,[\mu(\mu + \delta)(\mu + \mu_1 + r_1 + \eta)(1 - R_0)] + (\theta_3\eta + \theta_4 r_1)\mu(\mu + \delta) \\
&- f'(0)\mu(\mu + \delta)[\theta_2(\mu + \mu_1 + r_1 + \eta) - \theta_3\eta - \theta_4 r_1].
\end{aligned}
$$

Here, it is known that $\theta_1 = \theta_2 = \frac{\Pi}{\mu}$, and for sufficiently small $\varepsilon_1, \varepsilon_2 > 0$, we define

$$
\theta_3 = \frac{\theta_1}{2\eta}(\mu + \mu_1 + r_1 + \eta)(1 - R_0) - \varepsilon_1, \quad \theta_4 = \frac{\theta_1}{2r_1}(\mu + \mu_1 + r_1 + \eta)(1 - R_0) - \varepsilon_2, \quad \theta_5 = \Pi.
$$

Therefore,

$$
-\theta_1\,[\mu(\mu + \delta)(\mu + \mu_1 + r_1 + \eta)(1 - R_0)] + (\theta_3\eta + \theta_4 r_1)\mu(\mu + \delta) = -\mu(\mu + \delta)(\eta\varepsilon_1 + r_1\varepsilon_2),
$$

$$
\theta_2(\mu + \mu_1 + r_1 + \eta) - \theta_3\eta - \theta_4 r_1 = \theta_1(\mu + \mu_1 + r_1 + \eta)R_0 + (\varepsilon_1 + \varepsilon_2).
$$

To summarize the above analysis, we have

$$
\begin{aligned}
D_t^\alpha V_0 &\le -\mu(S - S_0)^2 + \frac{[\theta_1\Pi - (S - S_0)^2]\beta I}{f(I)(\mu + \delta)} + \xi(S - S_0)R \\
&- (\theta_1\mu - \theta_5)E - (\theta_1\delta - \theta_2\delta + \theta_5)E(t-\tau) - [\theta_3(\mu + \mu_2 + r_2) - \theta_4 r_2]\, H \\
&- \theta_4(\mu + \xi)R + \frac{\theta_1\beta\Pi\delta - \mu f(I)(\mu + \delta)(\theta_2(\mu + \mu_1 + r_1 + \eta) - \theta_3\eta - \theta_4 r_1)}{\mu f(I)(\mu + \delta)} \\
&\le -\mu(S - S_0)^2 + \frac{[\theta_1\Pi - (S - S_0)^2]\beta I}{f(I)(\mu + \delta)} + \xi(S - S_0)R
\end{aligned}
$$

$$
\begin{aligned}
&- \theta_5 E(t-\tau) - [\theta_3(\mu+\mu_2+r_2) - \theta_4 r_2]H - \theta_4(\mu+\xi)R \\
&- \frac{\mu(\mu+\delta)(\eta\varepsilon_1 + r_1\varepsilon_2) + \mu(\mu+\delta)[\theta_1(\mu+\mu_1+r_1+\eta)R_0 + (\varepsilon_1+\varepsilon_2)]}{\mu f(I)(\mu+\delta)}.
\end{aligned}
$$

For nonnegative values of S, E, I, H, and R, the above equation satisfies the conditions outlined in assumption (11). Consequently, we have $D_t^\alpha V_0 \leq 0$, with equality $D_t^\alpha V_0 = 0$ occurring only when $S = \frac{\Pi}{\mu}$ and $E = I = H = R = 0$.

Case 2: When $R_0 = 1$, based on the analysis of Case 1, we can define

$$
\theta_1 = \theta_2 = \frac{\Pi}{\mu}, \theta_3 = \theta_4 = 0, \theta_5 = \Pi.
$$

Therefore, for the expression, we have

$$
\begin{aligned}
&\theta_1\beta\Pi\delta - \mu f(I)(\mu+\delta)(\theta_2(\mu+\mu_1+r_1+\eta) - \theta_3\eta - \theta_4 r_1) \\
&\leq -\theta_1[\mu(\mu+\delta)(\mu+\mu_1+r_1+\eta)(1-R_0)] + (\theta_3\eta + \theta_4 r_1)\mu(\mu+\delta) \\
&- f'(0)\mu(\mu+\delta)[\theta_2(\mu+\mu_1+r_1+\eta) - \theta_3\eta - \theta_4 r_1] \\
&= -\Pi(\mu+\delta)(\mu+\mu_1+r_1+\eta)(1-R_0) - \Pi(\mu+\delta)(\mu+\mu_1+r_1+\eta) \\
&= -\Pi(\mu+\delta)(\mu+\mu_1+r_1+\eta).
\end{aligned}
$$

Then

$$
\begin{aligned}
D_t^\alpha V_0 \leq{}& -\mu(S-S_0)^2 + \frac{[\theta_1\Pi - (S-S_0)^2]\beta I}{f(I)(\mu+\delta)} + \xi(S-S_0)R - \theta_5 E(t-\tau) \\
&- \frac{\Pi(\mu+\delta)(\mu+\mu_1+r_1+\eta)}{\mu f(I)(\mu+\delta)}.
\end{aligned}
$$

For nonnegative S, E, I, H, R, the above equation satisfies the condition assumption (11); accordingly, we obtain $D_t^\alpha V_0 \leq 0$, with $D_t^\alpha V_0 = 0$ holding true only when $S = \frac{\Pi}{\mu}$ and $E = I = H = R = 0$.

To summarize the two cases, based on LaSalle's invariance principle [40], prerequisites for global asymptotic stability described in Theorem 4.4 are satisfied. □

Theorem 3.5 *If $R_0 > 1$, the endemic equilibrium $\epsilon_* = (S^*, E^*, I^*, H^*, R^*)$ is globally and asymptotically stable in system* (2).

Proof Construct the Lyapunov function

$$
\begin{aligned}
V_1(t) &= S - S^*(1 - \ln\frac{S}{S^*}), \\
V_2(t) &= E - E^*(1 - \ln\frac{E}{E^*}), \\
V_3(t) &= I - I^*(1 - \ln\frac{I}{I^*}), \\
V_4(t) &= H - H^*(1 - \ln\frac{H}{H^*}),
\end{aligned}
$$

$$V_5(t) = R - R^*(1 - \ln \frac{R}{R^*}).$$

Deriving the fractional derivative of the previous equations based on system (2) gives

$$\begin{aligned} D_t^\alpha V_1(t) &\le \left(1 - \frac{S^*}{S}\right)\left(\Pi - \mu S - \frac{\beta SI}{1+mI} + \xi R(t)\right) \\ &= \mu S^*\left(2 - \frac{S}{S^*} - \frac{S^*}{S}\right) + \frac{\beta S^* I^*}{1+mI^*}\left(1 - \frac{S^*}{S} + \frac{1+mI^*}{1+mI}\left(\frac{I}{I^*} - \frac{SI}{S^*I^*}\right)\right) \\ &\quad + \xi R^*\left(1 + \frac{R}{R^*} - \frac{S^*}{S} - \frac{R}{R^*}\frac{S^*}{S}\right), \end{aligned}$$

$$\begin{aligned} D_t^\alpha V_2(t) &\le \left(1 - \frac{E^*}{E}\right)\left(\frac{\beta SI}{1+mI} - \mu E - \delta E\right) \\ &= \frac{\beta S^* I^*}{1+mI^*}\left(1 - \frac{E}{E^*} + \frac{1+mI^*}{1+mI}\frac{SI}{S^*I^*} - \frac{E^*}{E}\frac{1+mI^*}{1+mI}\frac{SI}{S^*I^*}\right), \end{aligned}$$

$$\begin{aligned} D_t^\alpha V_3(t) &\le \left(1 - \frac{I^*}{I}\right)(\delta E(t) - (\mu + \mu_1 + r_1 + \eta)I) \\ &= (\mu + \mu_1 + r_1 + \eta)\left(1 - \frac{I^*}{I} - \frac{E}{E^*}\frac{I^*}{I} + \frac{E}{E^*}\right)I^*, \end{aligned}$$

$$\begin{aligned} D_t^\alpha V_4(t) &\le \left(1 - \frac{H^*}{H}\right)(\eta I - (\mu + \mu_2 + r_2)H) \\ &= (\mu + \mu_2 + r_2)\left(1 + \frac{1}{I^*} - \frac{H}{H^*} - \frac{1}{I^*}\frac{H}{H^*}\right)H^*, \end{aligned}$$

$$\begin{aligned} D_t^\alpha V_5(t) &\le \left(1 - \frac{R^*}{R}\right)(r_1 I + r_2 H - (\mu + \xi)R) \\ &= r_1 I^*\left(1 + \frac{I}{I^*} - \frac{R^* I}{RI^*} - \frac{R}{R^*}\right) + r_2 H^*\left(1 + \frac{H}{H^*} - \frac{R}{R^*} - \frac{R^* H}{RH^*}\right). \end{aligned}$$

Using the arithmetic-geometric mean inequality [45], we have

$$\begin{aligned} &2 - \frac{S}{S^*} - \frac{S^*}{S} \le 0, \quad 1 - \frac{S^*}{S} + \frac{1+mI^*}{1+mI}\left(\frac{I}{I^*} - \frac{SI}{S^*I^*}\right) \le 0, \\ &1 + \frac{R}{R^*} - \frac{S^*}{S} - \frac{R}{R^*}\frac{S^*}{S} \le 0, \quad 1 - \frac{E}{E^*} - \frac{E^*}{E}\frac{1+mI^*}{1+mI}\frac{SI}{S^*I^*} + \frac{1+mI^*}{1+mI}\frac{SI}{S^*I^*} \le 0, \\ &1 - \frac{I^*}{I} - \frac{E}{E^*}\frac{I^*}{I} + \frac{E}{E^*} \le 0, \quad 1 + \frac{1}{I^*} - \frac{H}{H^*} - \frac{1}{I^*}\frac{H}{H^*} \le 0, \\ &1 + \frac{I}{I^*} - \frac{R^* I}{RI^*} - \frac{R}{R^*} \le 0, \quad 1 + \frac{H}{H^*} - \frac{R}{R^*} - \frac{R^* H}{RH^*} \le 0. \end{aligned}$$

Then we can obtain

$$D_t^\alpha V \le D_t^\alpha V_1 + D_t^\alpha V_2 + D_t^\alpha V_3 + D_t^\alpha V_4 + D_t^\alpha V_5 \le 0. \tag{12}$$

Moreover, $D_t^{\alpha} V = 0$ occurs exclusively when $S = S^*, E = E^*, I = I^*, H = H^*, R = R^*$. Utilizing LaSalle's invariance principle [40], prerequisites for global asymptotic stability described in Theorem 4.5 are satisfied. □

3.6 Hopf bifurcation analysis

In this subsection, we now proceed to investigating the conditions under which a local bifurcation may occur at the endemic equilibrium $\epsilon_* = (S^*, E^*, I^*, H^*, R^*)$ of system (2). At the equilibrium ϵ_*, the characteristic equation for system (2) is given

$$\lambda^5 + a_4\lambda^4 + a_3\lambda^3 + a_2\lambda^2 + a_1\lambda + a_0 + (b_4\lambda^4 + b_3\lambda^3 + b_2\lambda^2 + b_1\lambda + b_0)e^{-\lambda\tau} = 0, \tag{13}$$

where

$$\begin{aligned}
a_4 &= A + C + D + E + 2\mu,\\
a_3 &= \mu^2 + AC + AE + CD + CE + AD + DE + A\mu + 2\mu C + 2\mu D + 2\mu E,\\
a_2 &= C\mu^2 + D\mu^2 + E\mu^2 + ACD + ACE + ADE + CDE + AC\mu + AD\mu + AE\mu\\
&\quad + 2CD\mu + 2CE\mu + 2DE\mu,\\
a_1 &= CD\mu^2 + CE\mu^2 + DE\mu^2 + ACDE + ACD\mu + ACE\mu + ADE\mu + 2CDE\mu,\\
a_0 &= CDE\mu^2 + ACDE\mu, b_4 = \delta, b_3 = A\delta - B\delta + C\delta + D\delta + E\delta + \delta\mu,\\
b_2 &= AC\delta + AD\delta + AE\delta - BD\delta - BE\delta + CD\delta + CE\delta + DE\delta - B\delta\mu + C\delta\mu\\
&\quad + D\delta\mu + E\delta\mu,\\
b_1 &= -BD\delta\mu - BE\delta\mu + CD\delta\mu + CE\delta\mu + DE\delta\mu - A\delta r_1\xi + ACD\delta + ACE\delta + ADE\delta\\
&\quad - BDE\delta + CDE\delta,\\
b_0 &= -AD\delta r_1\xi - A\delta\eta r_2\xi + ACDE\delta - BDE\delta\mu + CDE\delta\mu
\end{aligned}$$

with $A = \frac{\beta I^*}{1+mI^*}$; $B = \frac{\beta S^*}{(1+mI^*)^2}$; $C = \mu + \mu_1 + r_1 + \eta$; $D = \mu + \mu_2 + r_2$; and $E = \mu + \xi$.

Case 1: Assume that when $\tau = 0$, equation (13) transforms into

$$\lambda^5 + \nu_4\lambda^4 + \nu_3\lambda^3 + \nu_2\lambda^2 + \nu_1\lambda + \nu_0 = 0, \tag{14}$$

where $\nu_1 = b_1 + a_1$, $\nu_2 = b_2 + a_2$, $\nu_3 = b_3 + a_3$, $\nu_4 = b_4 + a_4$, $\nu_0 = a_0 + b_0$. Obviously, $\nu_4 = A + C + D + E + 2\mu + \delta > 0$, let $\Delta_1 = \nu_4 > 0$. As a result, by applying the Routh–Hurwitz criterion [43, 44], the following expressions are obtained:

$$\Delta_2 = \begin{vmatrix} \nu_4 & \nu_2 \\ 1 & \nu_3 \end{vmatrix} = \nu_3\nu_4 - \nu_2 > 0, \tag{15}$$

$$\Delta_3 = \begin{vmatrix} \nu_4 & \nu_2 & \nu_0 \\ 1 & \nu_3 & \nu_1 \\ 0 & \nu_4 & \nu_2 \end{vmatrix} = \nu_4 \begin{vmatrix} \nu_3 & \nu_1 \\ \nu_4 & \nu_2 \end{vmatrix} = \nu_4(\nu_3\nu_2 - \nu_4\nu_1) > 0, \tag{16}$$

$$\Delta_4 = \begin{vmatrix} \nu_4 & \nu_2 & \nu_0 & 0 \\ 1 & \nu_3 & \nu_1 & 0 \\ 0 & \nu_4 & \nu_2 & \nu_0 \\ 0 & 1 & \nu_3 & \nu_1 \end{vmatrix} > 0, \tag{17}$$

$$\Delta_5 = \begin{vmatrix} \nu_4 & \nu_2 & \nu_0 & 0 & 0 \\ 1 & \nu_3 & \nu_1 & 0 & 0 \\ 0 & \nu_4 & \nu_2 & \nu_0 & 0 \\ 0 & 1 & \nu_3 & \nu_1 & 0 \\ 0 & 0 & \nu_4 & \nu_2 & \nu_0 \end{vmatrix} > 0. \tag{18}$$

According to the analysis of the above theoretical steps, if the requirements specified in equations (15)–(18) are met, then system (2) without delay demonstrates local asymptotic stability at the endemic equilibrium E_*.

Case 2: In the case where $\tau \neq 0$, let $\lambda = i\omega(\omega > 0)$ be a root of expression (13). We substitute it into the equation. By distinguishing between the real and imaginary parts, we have

$$\begin{cases} N_3(\omega) = N_1(\omega)\cos(\tau\omega) - N_2(\omega)\sin(\tau\omega), \\ N_6(\omega) = N_5(\omega)\cos(\tau\omega) + N_4(\omega)\sin(\tau\omega), \end{cases} \tag{19}$$

where

$$N_1(\omega) = b_1 - b_3\omega^2, N_2(\omega) = b_2\omega - b_4\omega^3, N_3(\omega) = a_4\omega^4 + a_2\omega^2 - a_0,$$
$$N_4(\omega) = b_3\omega^2 - b_1, N_5(\omega) = b_2\omega + b_4\omega^3, N_6(\omega) = \omega^5 - a_3\omega^3 + a_1\omega.$$

Further, according to equation (19), we have

$$\cos(\omega\tau) = \frac{k_8\omega^8 + k_7\omega^7 + k_6\omega^6 + k_5\omega^5 + k_4\omega^4 + k_3\omega^3 + k_2\omega^2 + k_1\omega}{p_6\omega^6 + p_5\omega^5 + p_3\omega^3}, \tag{20}$$

$$\sin(\omega\tau) = \frac{q_8\omega^8 + q_7\omega^7 + q_6\omega^6 + q_5\omega^5 + q_4\omega^4 + q_3\omega^3 + q_2\omega^2 + q_1\omega}{m_5\omega^5 + m_4\omega^4 + m_3\omega^3 + m_1\omega + m_0} \tag{21}$$

with

$$k_8 = -b_4, k_7 = a_4b_4, k_6 = b_2 - b_4a_3, k_5 = a_4b_2 + a_2b_4,$$
$$k_4 = a_2b_2 - b_4a_1, k_3 = -a_0b_4 + b_2a_1, k_2 = a_2b_2, k_1 = -a_0b_2,$$
$$p_6 = -2b_3b_4, p_5 = -2b_3b_4, p_3 = 2b_1b_4,$$
$$q_8 = -a_4b_4, q_7 = -a_2b_4 - b_3, q_6 = -a_2b_4, q_5 = b_1 - a_4b_2,$$
$$q_4 = a_1b_1 - a_0b_2, q_3 = a_1b_1, q_2 = a_1b_1,$$
$$m_5 = -b_4b_3, m_4 = b_3^2, m_3 = b_2b_3 + b_4b_1, m_1 = -b_2b_1, m_0 = -b_1^2.$$

Since $\sin^2(\omega\tau) + \cos^2(\omega\tau) = 1$, we have

$$d_{16}\omega^{16} + d_{15}\omega^{15} + d_{14}\omega^{14} + \cdots + d_2\omega^2 + d_1\omega + d_0 = 0, \tag{22}$$

where

$$
\begin{aligned}
&d_{16} = k_8^2 + q_8^2, d_{15} = 2k_8k_7 + 2q_8q_7, d_{14} = 2k_8k_6 + k_7^2 + 2q_8q_6 + q_7^2,\\
&d_{13} = 2k_8k_5 + 2k_7k_6 + 2q_8q_5 + 2q_7q_6,\\
&d_{12} = 2k_8k_4 + 2k_7k_5 + k_6^2 + 2q_8q_4 + 2q_7q_5 + q_6^2 - p_6^2m_5^2,\\
&d_{11} = 2k_8k_3 + 2k_7k_4 + 2k_6k_5 + 2q_8q_3 + 2q_7q_4 + 2q_6q_5 - 2p_6p_5m_5^2,\\
&d_{10} = 2k_8k_2 + 2k_7k_3 + 2k_6k_4 + k_5^2 + 2q_8q_2 + 2q_7q_3 + 2q_6q_4 + q_5^2\\
&\quad - (p_5^2m_5^2 + 2p_6p_3m_5^2 + 2p_6p_5m_4m_5),\\
&d_9 = 2k_8k_1 + 2k_7k_2 + 2k_6k_3 + 2k_5k_4 + 2q_8q_1 + 2q_7q_2 + 2q_6q_3 + 2q_5q_4\\
&\quad - 2(p_5p_3m_5^2 + p_6p_3m_4m_5 + p_6p_5m_3m_5),\\
&d_8 = k_7^2 + 2k_8k_0 + 2k_6k_2 + 2k_5k_3 + k_4^2 + q_7^2 + 2q_8q_0 + 2q_6q_2 + 2q_5q_3 + q_4^2\\
&\quad - (p_5^2m_4^2 + 2p_3p_6m_3m_4 + p_6^2m_2m_3),\\
&d_7 = 2k_7k_1 + 2k_6k_2 + 2k_5k_3 + 2q_7q_1 + 2q_6q_2 + 2q_5q_3 - 2(p_5p_3m_3 + p_6p_3m_2),\\
&d_6 = 2k_6k_0 + 2k_5k_1 + 2q_6q_0 + 2q_5q_1 - 2(p_5p_3m_2 + p_6^2m_0), d_5 = 2k_5k_0 + 2q_5q_0 - 2p_5m_0,\\
&d_4 = k_4^2 + q_4^2 - p_5^2m_0, d_3 = 2k_3k_1 + q_3^2 + 2q_3q_1 - p_3^2m_0, d_2 = k_1^2 + q_1^2 - p_2^2m_2.
\end{aligned}
$$

We now introduce the following assumptions: if equation (20) possesses a positive root ω_0, then expression (13) will have a completely imaginary root given by $i\omega_0$. Thus, the critical threshold for the delay τ in relation to ω_0 can be identified as

$$
\tau_0 = \frac{\arccos\left(\frac{k_8\omega_0^8 + k_7\omega_0^7 + k_6\omega_0^6 + k_5\omega_0^5 + k_4\omega_0^4 + k_3\omega_0^3 + k_2\omega_0^2 + k_1\omega_0}{p_6\omega_0^6 + p_5\omega_0^5 + p_3\omega_0^3}\right)}{\omega_0}. \tag{23}
$$

Moreover, applying differentiation to both sides of equation (13) regarding τ yields

$$
\left[\frac{d\lambda}{d\tau}\right]^{-1} = \frac{O(\lambda)}{V(\lambda)} - \frac{\tau}{\lambda}, \tag{24}
$$

where

$$
\begin{aligned}
&O(\lambda) = b_4\lambda^5 + b_3\lambda^4 + b_2\lambda^3 + b_1\lambda^2 + b_0\lambda,\\
&V(\lambda) = 5\lambda^4 + 4a_4\lambda^3 + 3a_3\lambda^2 + 2a_2\lambda + a_1 + (4b_4\lambda^3 + 3b_3\lambda^2 + 2b_2\lambda + b_1)e^{-\lambda\tau}.
\end{aligned}
$$

Define

$$
\mathrm{Re}\left[\left(\frac{d\lambda}{d\tau}\right]^{-1}\right]_{\tau=\tau_0} = \frac{\mathrm{Im}(O)\mathrm{Im}(V) + \mathrm{Re}(V)\mathrm{Re}(O)}{\mathrm{Im}(V)^2 + \mathrm{Re}(V)^2}.
$$

Clearly, if the condition $\mathrm{Im}(O)\mathrm{Im}(V) + \mathrm{Re}(V)\mathrm{Re}(O) \neq 0$ is satisfied, then $\mathrm{Re}\left[\left(\frac{d\lambda}{d\tau}\right]^{-1}\right]_{\tau=\tau_0} \neq 0$. Building on the preceding analysis and the Hopf bifurcation theory discussed in [28, 46], the following conclusion can be drawn.

Theorem 3.6 *Given that the condition* $\frac{Re(V)Re(O)+Im(O)Im(V)}{Im(V)^2+Re(V)^2} \neq 0$ *is satisfied, the following conclusions hold*:

(i) *The equilibrium* $\epsilon_* = (S^*, E^*, I^*, H^*, R^*)$ *of system* (2) *is asymptotically stable when* τ *lies within the interval* $[0, \tau_0)$.

(ii) *When* $\tau = \tau_0$, *system* (2) *experiences a Hopf bifurcation at the equilibrium* $\epsilon_* = (S^*, E^*, I^*, H^*, R^*)$.

Here, τ_0 *is as defined in equation* (23).

4 Numerical simulation

In this section, we perform computational simulations to explore the dynamic behavior of system (2). Due to the complexity of obtaining an explicit analytical solution, numerical methods are essential for the analysis. Using MATLAB R2018b, we visually demonstrate the theoretical results presented earlier, with the initial conditions set as $S_0 = 5$, $E_0 = 1$, $I_0 = 2$, $H_0 = 1$, and $R_0 = 1$. Various parameter configurations are explored to examine different dynamic scenarios. The Adams–Bashforth–Moulton method, implemented in MATLAB [22, 47], is used to adjust the fractional order α, time delay τ, and inhibition parameter m, allowing us to observe their effects on the system, particularly in relation to the dynamics of susceptible and infected populations under varying conditions.

In our simulations, the initial values are set based on typical epidemiological data and real-world scenarios. For example, the initial number of infected individuals in certain compartments is relatively low (usually set to 1 or 10) to reflect the early stages of an epidemic, while the initial value of susceptible individuals is typically set as a large proportion of the total population.

Case 1: Dynamic analysis of system (2) with variable orders and distinct initial conditions.

This analysis investigates the behavior of system (2) at the disease-free equilibrium. The stability analysis (Fig. 2) shows that $R_0 = 0.6412 < 1$, indicating a stable disease-free equilibrium, meaning the disease will eventually subside. The dynamics, peak amplitudes, and rates in each compartment are affected by different values of α, with weaker transmission leading to a more manageable disease-free state.

The fractional order α also influences the system's memory effect. For instance, when $\alpha = 0.75$, the peak values for the compartments E (Fig. 2 (b)) and I (Fig. 2 (c)) are higher, and the return to equilibrium is slower, suggesting that earlier transmission has a stronger lingering effect, leading to a prolonged infection period. In contrast, when $\alpha = 1$, the system stabilizes more rapidly with lower peak values, indicating better control over the disease. Thus, a larger α reduces the impact of past events, facilitating a quicker return to equilibrium.

For the scenario where $R_0 = 1.9338 > 1$ (Fig. 3), the system reaches an endemic equilibrium with ongoing disease spread. Different values of α influence the long-term dynamics. Specifically, $\alpha = 0.75$ results in higher peaks for the compartments E (Fig. 3 (b)) and I (Fig. 3 (c)), indicating prolonged exposure and infection periods, which complicate disease control efforts. On the other hand, when $\alpha = 1$, the system responds more swiftly, with shorter peaks, suggesting improved control over the disease spread. Larger values of α reduce the influence of historical dynamics, allowing for quicker stabilization at the endemic equilibrium.

In Fig. 4, where $R_0 < 1$, the disease cannot sustain itself, leading to a disease-free equilibrium. Regardless of the initial conditions, the compartments S, E, and H all converge

toward the disease-free equilibrium ϵ_0, with a decline in S and reductions in both E and H, ultimately stabilizing in a disease-free state. In contrast, Fig. 5 shows that when $R_0 > 1$, the disease persists, reaching an endemic equilibrium. Despite variations in initial values, all trajectories converge toward the same endemic point ϵ^*, indicating that when $R_0 > 1$, the system stabilizes at a persistent level of infection. Overall, Figs. 4 and 5 further confirm the dynamic behavior of disease extinction and sustained transmission under different R_0 values, offering valuable simulation validation for the steady-state conditions described above.

Case 2: Dynamic analysis of system (2) under different inhibition factors (infection saturation parameter m) and delay effects τ.

As the inhibition factor or infection saturation parameter m increases, the dynamics of the system's compartments S, E, and R exhibit notable changes. In contrast, the dynamics of the I (infected) and H (isolated) compartments remain relatively stable under the current experimental conditions and do not significantly influence the overall system dynamics. Therefore, we did not prioritize their analysis. We believe that by focusing on the dynamics of the S, E, and R compartments, we have effectively captured the primary impact of the saturation control parameter m on disease transmission.

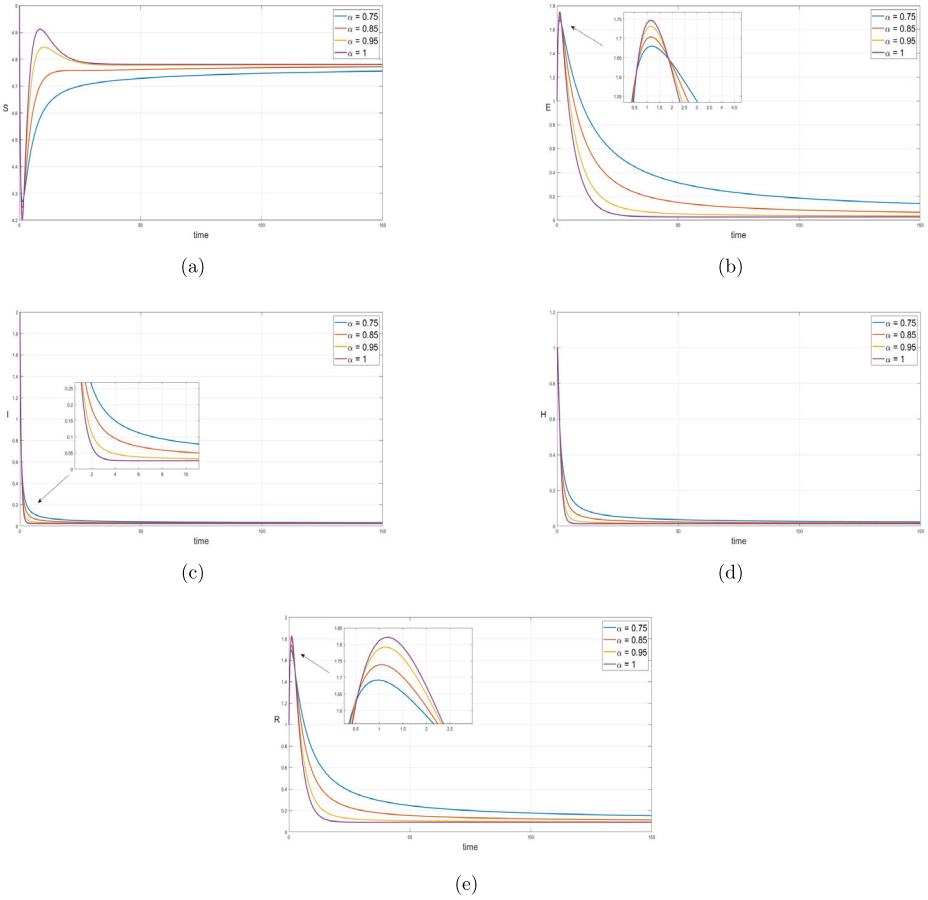

Figure 2 The dynamic behavior of system (2) at $R_0 = 0.6412 < 1$ for different orders $\boldsymbol{\alpha}$ and the parameter set $\Pi = 1$, $\beta = 0.45$, $\mu = 0.2$, $\delta = 0.3$, $\mu_1 = 0.35$, $\mu_2 = 0.15$, $r_1 = 0.7$, $r_2 = 0.8$, $\eta = 0.65$, $\xi = 0.125$, $m = 0.65$, and $\tau = 5$

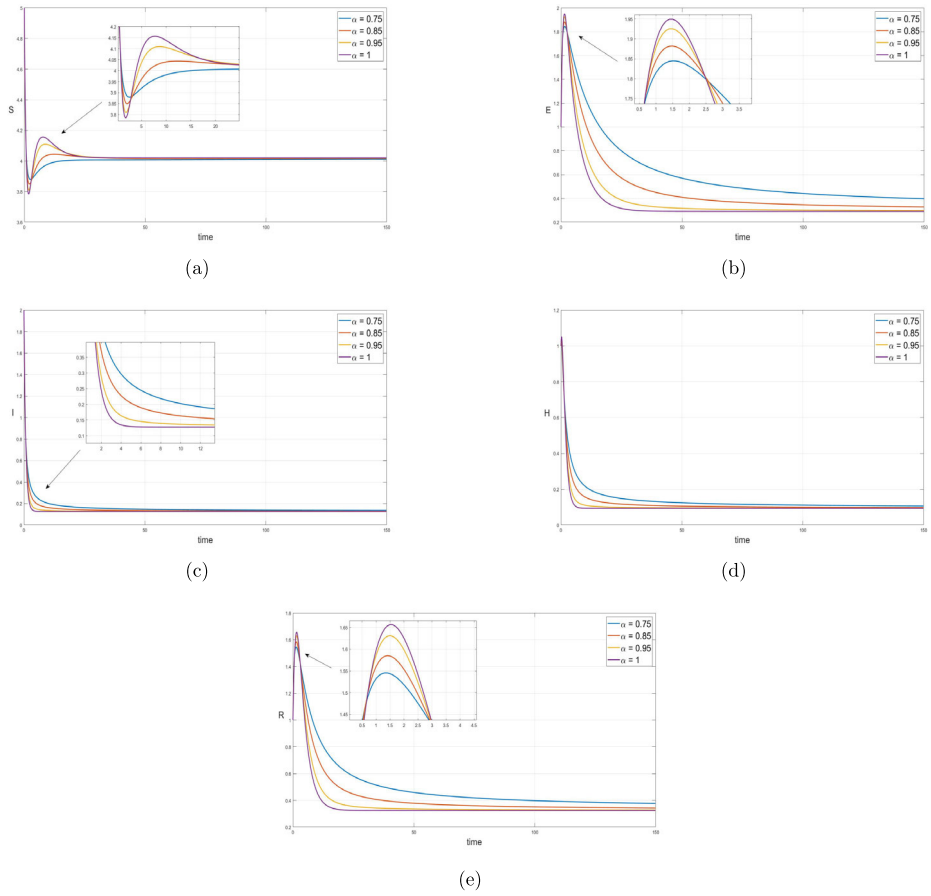

Figure 3 The dynamic behavior of system (2) at $R_0 = 1.9338 > 1$ for different orders α and the parameter set $\Pi = 1$, $\beta = 0.5$, $\mu = 0.2$, $\delta = 0.65$, $\mu_1 = 0.15$, $\mu_2 = 0.1$, $r_1 = 0.35$, $r_2 = 0.65$, $\eta = 0.7$, $\xi = 0.125$, $m = 0.65$, and $\tau = 3$

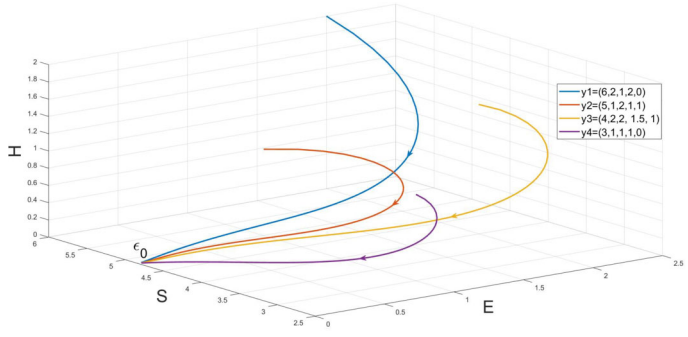

Figure 4 Phase plane analysis of system (2) with four different initial values ($y1$, $y2$, $y3$, $y4$) when $R_0 < 1$. The remaining parameter values are consistent with those in Fig. 2

In the susceptible compartment S (Fig. 6(a)), increasing m values result in a slower initial decrease in the susceptible group, eventually reaching a higher steady-state level. This implies that an increase in m reduces the infection rate, allowing more individuals to remain susceptible, thereby slowing the spread of infection.

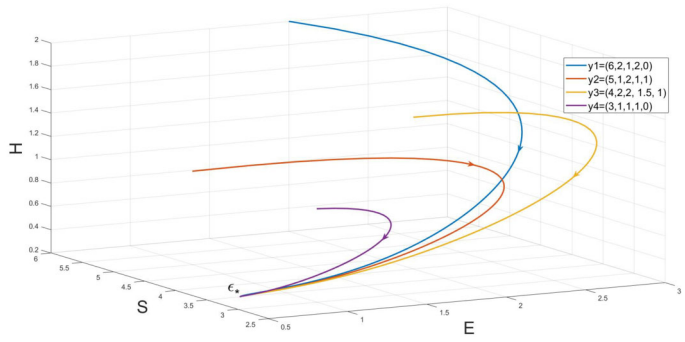

Figure 5 Phase plane analysis of system (2) with four different initial values ($y1$, $y2$, $y3$, $y4$) when $R_0 > 1$. The remaining parameter values are consistent with those in Fig. 3

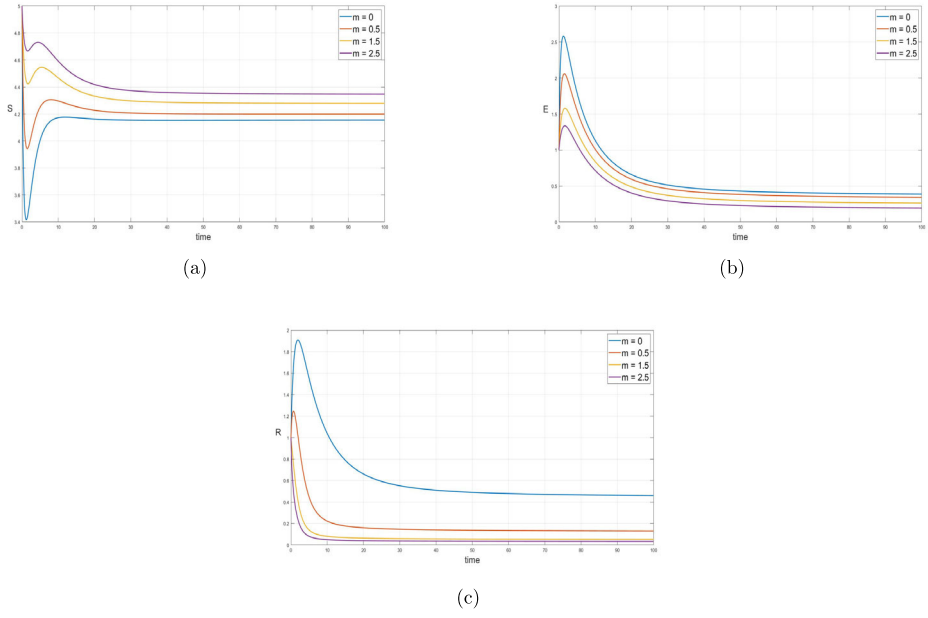

Figure 6 The dynamic behavior of system (2) for different infection saturation parameters m and the parameter set $\alpha = 0.95$, $\Pi = 1$, $\beta = 0.5$, $\mu = 0.2$, $\delta = 0.65$, $\mu_1 = 0.15$, $\mu_2 = 0.125$, $r_1 = 0.35$, $r_2 = 0.75$, $\eta = 0.7$, $\xi = 0.25$, and $\tau = 3$

In the exposed compartment E (Fig. 6(b)), higher m values result in a lower peak and faster decline, ultimately reaching a lower steady-state. This suggests that a stronger inhibition factor limits the accumulation of exposed individuals, thus restraining early transmission.

Similarly, in the recovered compartment R (Fig. 6(c)), higher m values lead to a lower peak and steady-state, indicating that increased infection saturation results in fewer recoveries. Therefore, larger m values inhibit transmission, reduce the accumulation of exposed and recovered individuals, and slow the spread of infection, helping the system achieve control and recovery more effectively.

In summary, the variation of the saturation inhibition parameter m reflects the impact of factors such as immune barriers, treatment and isolation measures, and resource limi-

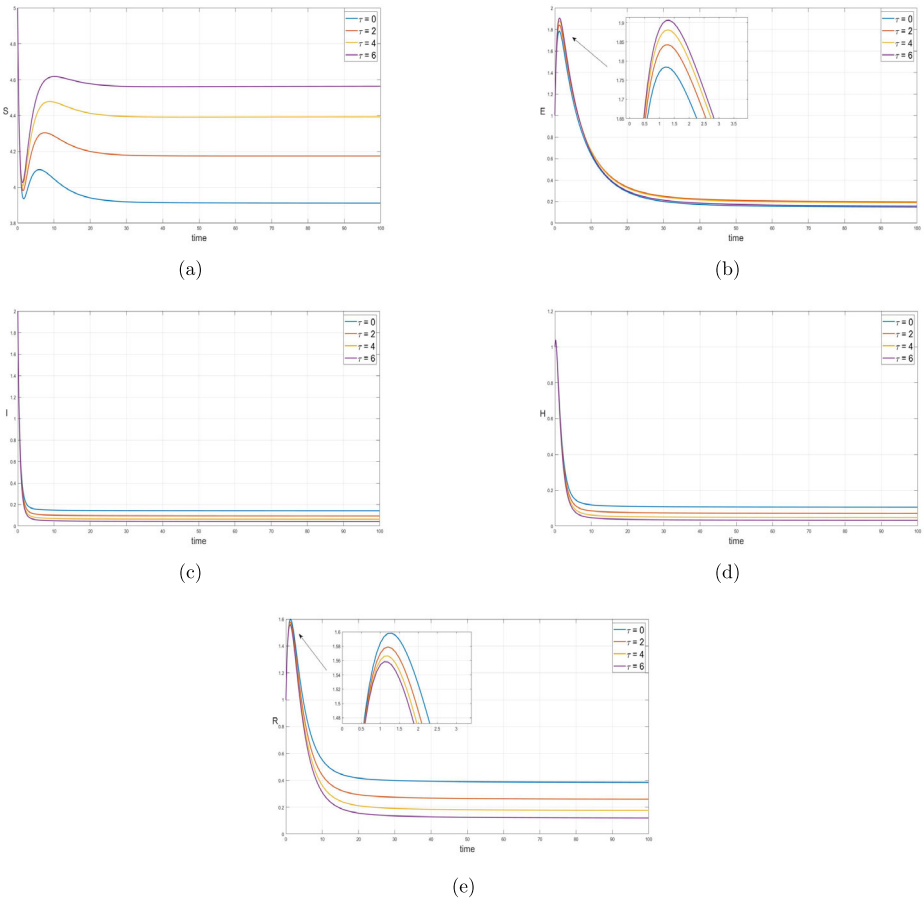

Figure 7 The dynamic behavior of system (2) for different time delay effects τ and the parameter set $\Pi = 1$, $\beta = 0.5$, $\mu = 0.2$, $\delta = 0.65$, $\mu_1 = 0.35$, $\mu_2 = 0.15$, $r_1 = 0.5$, $r_2 = 0.75$, $\eta = 0.7$, $\xi = 0.15$, $m = 0.75$, and $\alpha = 0.95$

tations. As the number of infected individuals increases, herd immunity effects or control measures begin to take effect, reducing the transmission rate of the disease. Additionally, as healthcare resources become strained, the efficiency of disease transmission is further limited. Through this parameter, the model quantifies the inhibitory effects of these factors on disease spread, allowing for a more accurate description of the epidemic's progression.

By adjusting the parameters, Fig. 7 illustrates how the delay parameter τ influences population dynamics. As τ increases, the adjustment rate across the compartments S, E, I, H, and R significantly slows down, with the most noticeable effect occurring at $\tau = 6$. Larger τ values result in a slower decline of S (Fig. 7(a)), a higher peak and longer duration for E (Fig. 7(b)), and a delayed reduction in I (Fig. 7(c)), indicating a slower response to early infection.

Moreover, the isolated compartment H (Fig. 7(d)) declines at a slower rate, suggesting decreased efficiency in isolation measures. The recovery of individuals in R (Fig. 7(e)) is also hindered, stabilizing at a lower level, which reflects delays in treatment and recovery. Overall, increasing delays reduce the system's responsiveness, prolong disease transmission and control, and complicate disease management. Thus, reducing τ to enable faster responses is crucial for effective disease containment and treatment.

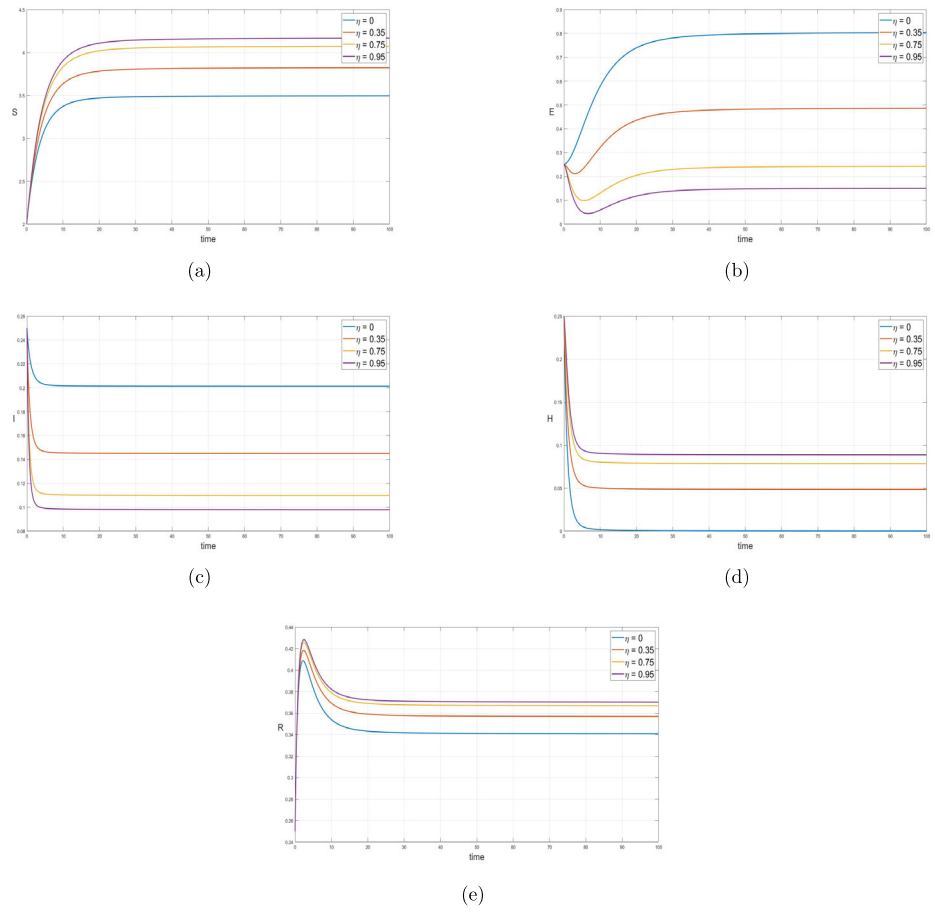

Figure 8 The dynamic behavior of system (2) for different hospitalization isolation rate η and the parameter set $\Pi = 1$, $\beta = 0.55$, $\mu = 0.2$, $\delta = 0.6$, $\mu_1 = 0.15$, $\mu_2 = 0.1$, $r_1 = 0.55$, $r_2 = 0.75$, $\xi = 0.125$, $m = 0.65$, $\tau = 3$, $S_0 = 2$, $E_0 = 0.25$, $I_0 = 0.25$, $H_0 = 0.25$, and $R_0 = 0.25$

Case 3: Dynamic analysis of system (2) under different hospitalization isolation rates η.

The numerical simulation results in this study show that the hospitalization isolation rate η has a significant impact on disease transmission. To examine the progression of the disease, and based on the analysis in Case 1 with different initial values, we set the initial values as $S_0 = 2$, $E_0 = 0.25$, $I_0 = 0.25$, $H_0 = 0.25$, and $R_0 = 0.25$, which do not influence the final steady state of the disease.

As shown in Fig. 8, as η increases from 0 to 0.95, the rate of decline in the susceptible population (Fig. 8(a)) slows down, and the final steady-state level significantly rises, indicating that more people remain uninfected. The peak and steady-state levels of the exposed population (Fig. 8(b)) decrease markedly with higher η; for example, when $\eta = 0$, the peak of the exposed population is close to 0.7, but it drops below 0.3 when $\eta = 0.95$. Similarly, the peak and duration of the infectious population (Fig. 8(c)) decrease as η increases. The initial peak of the hospitalized population (Fig. 8(d)) rises at higher values of η, but its steady-state level subsequently decreases. The total size of the recovered population (Fig. 8(e)) also decreases with higher isolation rates.

These numerical changes indicate that a higher isolation rate significantly reduces the sizes of the exposed, infectious, and recovered populations, effectively suppressing disease

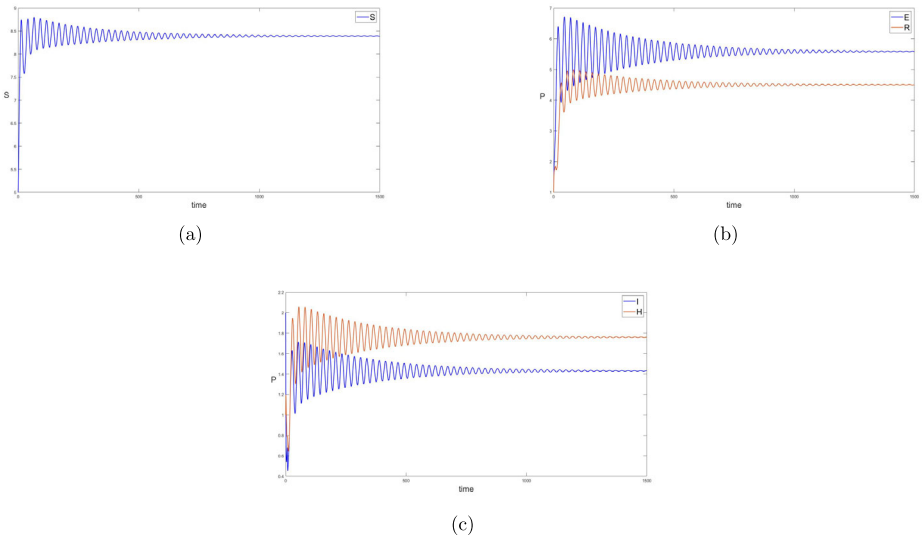

Figure 9 The time series of system (2) for $\alpha = 0.95$ and $\tau = 6.85$ with the following parameter values $\Pi = 1$, $\beta = 0.35$, $\mu = 0.02$, $\delta = 0.25$, $\mu_1 = 0.15$, $\mu_2 = 0.2$, $r_1 = 0.35$, $r_2 = 0.15$, $\eta = 0.455$, $\xi = 0.15$, and $m = 1.25$

transmission. Biologically, the isolation rate represents the proportion of infected individuals who are separated from the population, either through hospitalization or quarantine. By isolating infected individuals, disease transmission is reduced as they have less contact with susceptible individuals, helping to control outbreaks and prevent secondary infections. In highly contagious diseases, effective isolation is crucial for controlling spread and reducing the epidemic peak.

Case 4: Dynamic analysis of periodic oscillations in system (2) under different time delays.

By adjusting the parameter values of system (2) and conducting simulations, the results demonstrate how fractional-order dynamics and time delays impact both the steady-state and periodic responses.

In system (2) with an order of 0.95, increasing the time-delay parameter induces significant dynamic changes. As shown in Figs. 9–11, when the delay is set to $\tau = 6.95 < \tau_0$, the system achieves asymptotic stability at the endemic equilibrium. As the delay approaches this value, the limit cycle narrows and converges to a stable focus. However, as τ increases from 6.95 to 7.299, a Hopf bifurcation occurs, transitioning the system's stability from the equilibrium point to a periodic orbit. This indicates that once τ exceeds the critical threshold τ_0, stability is lost, and periodic oscillations emerge, as illustrated in Figs. 12–14. In Figs. 13 and 14, the system stabilizes into a periodic solution.

At a delay of $\tau = 7.85$ (beyond the critical threshold τ_0), the amplitude of oscillations increases, further compromising stability, as shown in Figs. 15–17. This Hopf bifurcation behavior is particularly significant in infectious disease modeling, as the onset of periodic oscillations highlights the necessity for timely interventions to manage transmission peaks effectively.

From a biological perspective, time delay reflects the gap between exposure to the pathogen and the onset of symptoms or treatment. This delay can lead to rapid disease spread before effective control measures, such as isolation or vaccination, can be implemented. Understanding the impact of time delays is crucial as even small changes in intervention timing can significantly affect the outbreak trajectory. Managing delay parameters

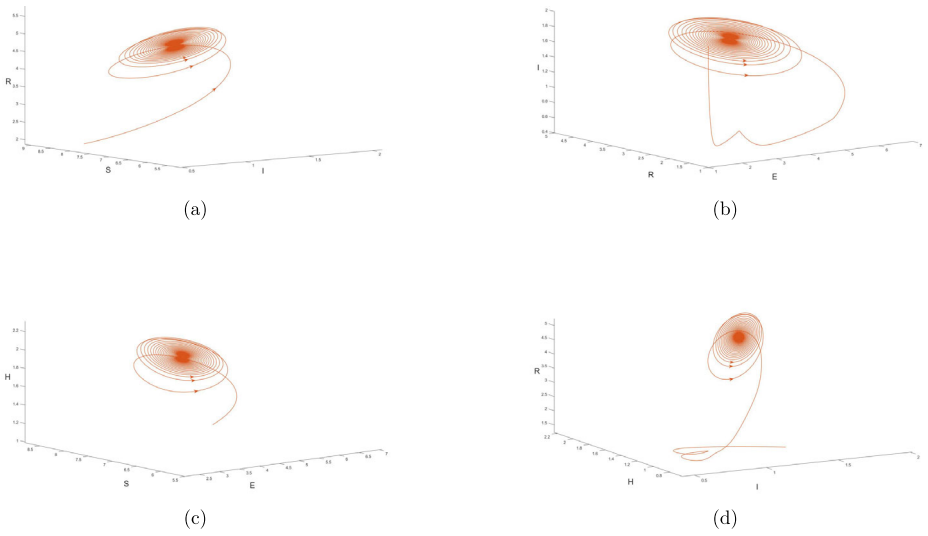

Figure 10 Attractor images for different state variables of system (2) with $\alpha = 0.95$ and $\tau = 6.85$. The remaining parameter values are consistent with those in Fig. 9

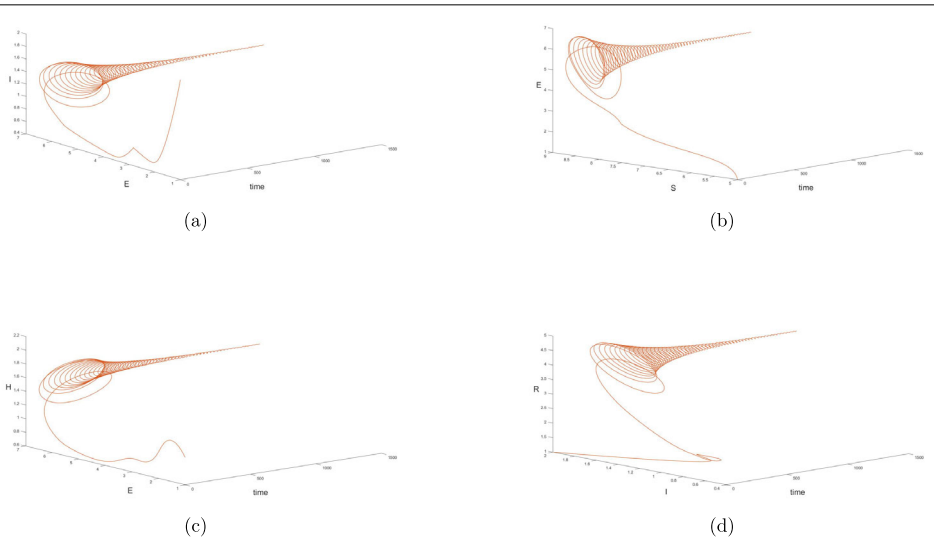

Figure 11 Projection of different state variables of system (2) with $\alpha = 0.95$ and $\tau = 6.85$. The remaining parameter values are consistent with those in Fig. 9

effectively allows for dynamic adjustments in transmission paths, improving model accuracy. In the context of antibiotic resistance, manipulating delay effects and monitoring oscillations can optimize resource allocation, enhance vaccination strategies, and ensure timely responses during transmission peaks, leading to more effective disease control.

Simulations reveal parameter-driven dynamic phenomena, where the system may either exhibit stable periodic behavior or transition to a stable equilibrium as key parameters vary. Notably, changes in initial conditions, transmission rates, inhibition levels, and delays can lead to a transition from stable periodic behavior to chaotic dynamics. Such chaotic behavior highlights the system's sensitivity to nonlinear interactions, behavioral shifts, and

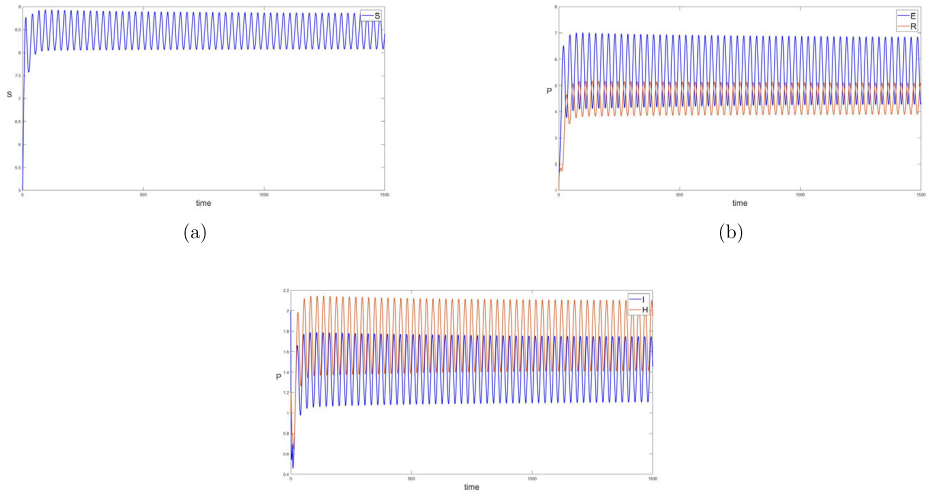

Figure 12 The time series of system (2) with $\alpha = 0.95$, $\tau = 7.299$. The remaining parameter values are consistent with those in Fig. 9

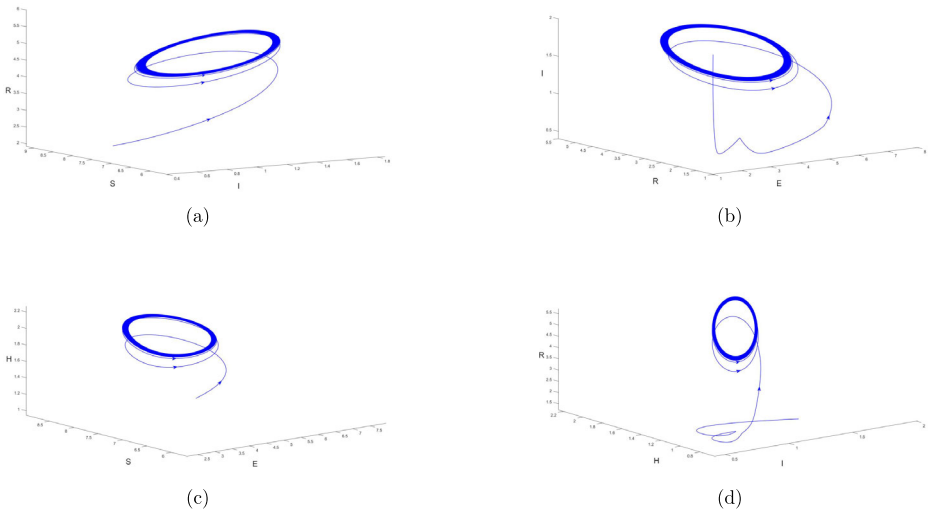

Figure 13 Attractor images for different state variables of system (2) with $\alpha = 0.95$, $\tau = 7.299$. The remaining parameter values are consistent with those in Fig. 9

environmental factors, emphasizing the complexities inherent in disease management and the unpredictable nature of transmission dynamics.

5 Conclusions

The rapid spread of infectious diseases presents a significant challenge in the field of public health, particularly during outbreaks of new diseases, which can quickly affect large populations and lead to widespread epidemics. To address this challenge, accurate infectious disease transmission models are crucial. Through mathematical modeling, we can simulate disease spread, predict epidemic trends, and evaluate the effectiveness of intervention measures. This paper proposes a new time-delay fractional-order SEIHR model aimed at

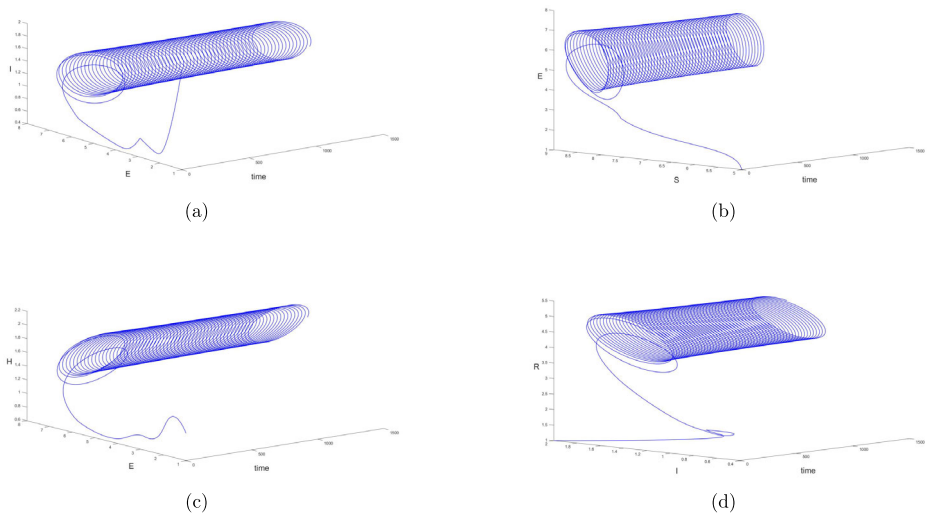

Figure 14 Projection of different state variables of system (2) with $\alpha = 0.95$, $\tau = 7.299$. The remaining parameter values are consistent with those in Fig. 9

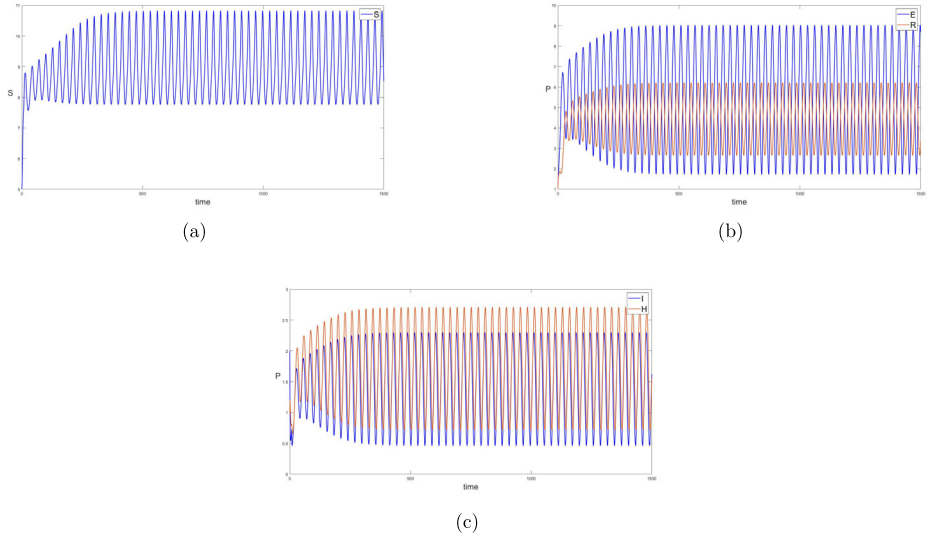

Figure 15 The time series of system (2) with $\alpha = 0.95$, $\tau = 7.85$. The remaining parameter values are consistent with those in Fig. 9

more accurately reflecting the complex process of infectious disease transmission. The model incorporates the traditional compartments of susceptible, exposed, infected, and recovered individuals, while also adding a hospitalized isolation compartment to simulate the effect of patient isolation in reducing transmission.

Additionally, the model accounts for time-delay effects under fractional-order dynamics, allowing for a more realistic representation of biological processes, particularly the interactions between disease spread and immune responses. Furthermore, the system introduces a nonlinear effect of saturated incidence rates. At high infection levels, as the number of infected individuals rises, the rate of contact between individuals progressively

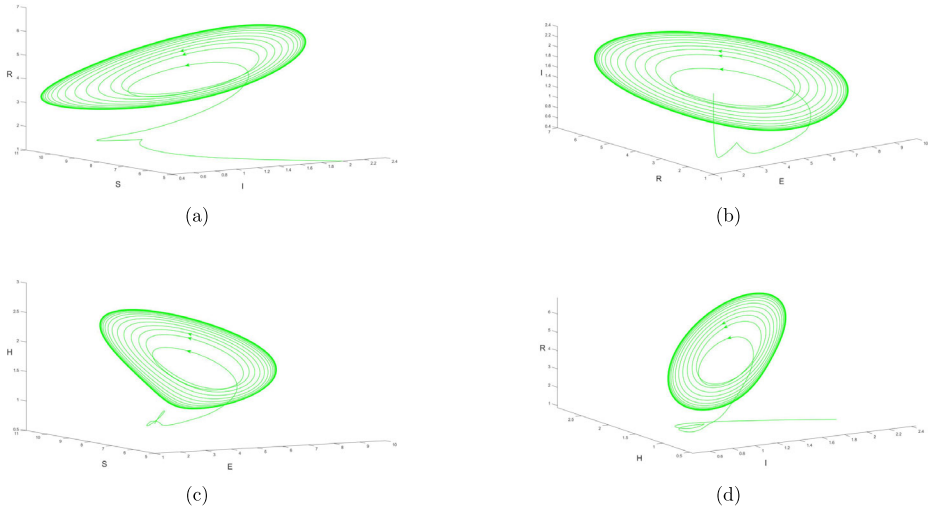

Figure 16 Attractor images for different state variables of system (2) with $\alpha = 0.95$, $\tau = 7.85$. The remaining parameter values are consistent with those in Fig. 9

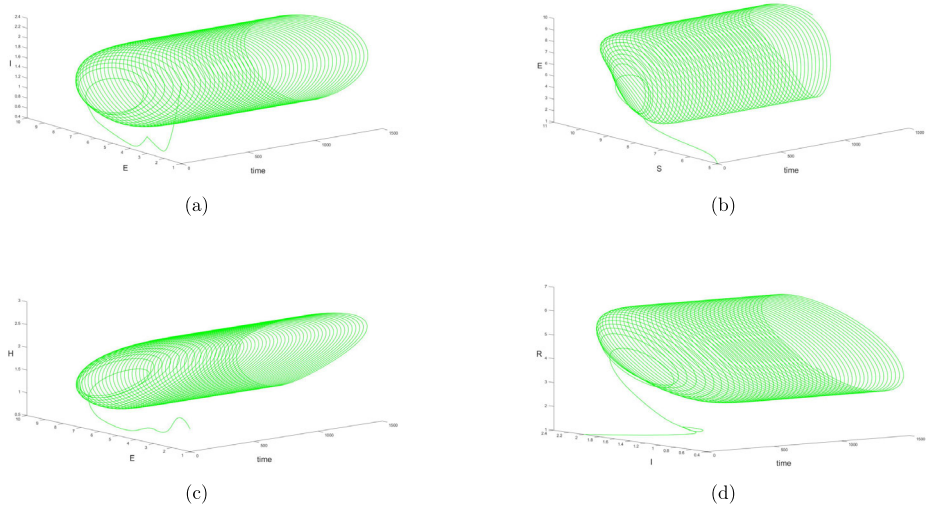

Figure 17 Projection of different state variables of system (2) with $\alpha = 0.95$, $\tau = 7.85$. The remaining parameter values are consistent with those in Fig. 9

declines, thereby slowing the spread of the disease. This effect enhances the system's realism, especially during large-scale epidemics, and aids in predicting the trends and extent of disease transmission.

First, we conducted a comprehensive analysis of the system's solution properties to ensure the biological feasibility of the system, proving the nonnegativity, uniqueness, and existence of the equilibria. These properties guarantee that the model can reasonably describe the disease transmission process, avoiding nonphysical solutions and ensuring the stability and consistency of the system. To validate the model's effectiveness, we applied the next-generation matrix technique to determine the basic reproduction number R_0, which reflects the disease's transmission potential. When $R_0 < 1$, the disease gradually

dies out, indicating that the transmission source is insufficient to trigger a large-scale epidemic. When $R_0 > 1$, the disease continues to spread, suggesting that the epidemic may proliferate.

Subsequently, using Lyapunov functions, we found that when $R_0 < 1$, the disease-free equilibrium is globally asymptotically stable, consistent with the biological expectation that control measures can eliminate the epidemic. In contrast, when $R_0 > 1$, the disease persists, and stronger control measures are required. Furthermore, the model accounts for the delay effects of the latent period. When the delay τ exceeds a critical value τ_0, the system exhibits periodic oscillations, leading to periodic solutions, as shown in Figs. 10–17. This reflects how infectious diseases with latent periods can capture the fluctuating nature of epidemic spread via time delays, causing different phases of disease transmission and control to exhibit varying patterns of outbreak and spread. By predicting the periodic fluctuations of the disease, we can more effectively intervene and control the epidemic.

Numerical simulations were used to validate the theoretical analysis, and the results showed significant phenomena of disease extinction or sustained transmission under different initial conditions and memory effects (denoted as α), as illustrated in Figs. 2–5, which confirm theoretical predictions. Additionally, as shown in Fig. 6, increasing the parameter m reduces the infection rate, allowing more individuals to remain susceptible and thereby slowing the transmission speed. As shown in Fig. 8, after introducing hospital isolation treatment, higher isolation rates (η) effectively reduced the population densities of exposed, infected, and recovered individuals, demonstrating the role of hospital isolation measures in controlling the disease.

Currently, the system only considers disease transmission factors prior to treatment and does not account for the dynamic changes in different populations after treatment. Future research will incorporate various treatment strategies, such as vaccination, mask-wearing, and government interventions, and apply optimal control theory to explore how to achieve the best control outcomes with minimal treatment costs under limited resources.

Author contributions
The main idea of this paper was proposed by WW and JZ. ZL initially prepared the manuscript and performed all the steps of the proofs in this research. WT provided the validation and acquired the funding. All authors read and approved the final manuscript.

Funding
This work was supported by the National Natural Science Foundation of China (Nos. 12361104, 12261104), Yunnan Fundamental Research Projects (grant NO. 202401AS070148), the Yunnan Provincial Basic Research Program Project (No. 202301AT070016, No. 202401AT070036), the Youth Talent Program of Xingdian Talent Support Plan (XDYCQNRC-2022-0514), and the Yunnan Province International Joint Laboratory for Intelligent Integration and Application of Ethnic Multilingualism (No. 202403AP140014).

Data availability
Not applicable
Materials availability
Not applicable

Code availability
Not applicable

Declarations

Competing interests
The authors have no conflicts to disclose.

Received: 11 November 2024 Accepted: 30 December 2024 Published online: 17 January 2025

References

1. Wu, Y., Zhang, Z., Song, L., Xia, C.: Global stability analysis of two strains epidemic model with imperfect vaccination and immunity waning in a complex network. Chaos Solitons Fractals **179**, 114414 (2024)
2. Saleem, S., Rafiq, M., Ahmed, N., Arif, M.S., Raza, A., Iqbal, Z., Niazai, S., Khan, I.: Fractional epidemic model of coronavirus disease with vaccination and crowding effects. Sci. Rep. **14**(1), 8157 (2024)
3. Federico, S., Ferrari, G., Torrente, M.-L.: Optimal vaccination in a SIRS epidemic model. Econ. Theory **77**(1), 49–74 (2024)
4. Biswas, S.K., Ghosh, U., Sarkar, S.: A mathematical model of Zika virus transmission with saturated incidence and optimal control: a case study of 2016 Zika outbreak in Puerto Rico. Int. J. Model. Simul. **44**(3), 172–189 (2024)
5. Huang, L., Qin, W., Chen, S.: Nonsmooth dynamics of a Filippov predator–prey ecological model with antipredator behavior. Adv. Cont. Discr. Mod. **2024**(1), 13 (2024)
6. Bentaleb, D., Harroudi, S., Amine, S., Allali, K.: Analysis and optimal control of a multistrain SEIR epidemic model with saturated incidence rate and treatment. Differ. Equ. Dyn. Syst. **31**(4), 907–923 (2023)
7. Qin, W., Dong, Z.: The impact of resource limitation on the pest-natural enemy ecosystem with anti-predator behavior and fear effect. Adv. Cont. Discr. Mod. **2024**(1), 10 (2024)
8. Dietz, K., Heesterbeek, J.: Daniel Bernoulli's epidemiological model revisited. Math. Biosci. **180**(1–2), 1–21 (2002)
9. Kermack, W.O., McKendrick, A.G.: A contribution to the mathematical theory of epidemics. Proc. R. Soc. Lond. Ser. A, Contain. Pap. Math. Phys. Character **115**(772), 700–721 (1927)
10. Barman, S., Jana, S., Majee, S., Das, D.K., Kar, T.K.: Complex dynamics of a fractional-order epidemic model with saturated media effect. Nonlinear Dyn. **112**(20), 18611–18637 (2024)
11. Lan, G., Song, B., Yuan, S.: Epidemic threshold and ergodicity of an SEIR model with vertical transmission under the telegraph noise. Chaos Solitons Fractals **167**, 113017 (2023)
12. Lan, X., Chen, G., Zhou, R., Zheng, K., Cai, S., Wei, F., Jin, Z., Mao, X.: An SEIHR model with age group and social contact for analysis of Fuzhou COVID-19 large wave. Infect. Dis. Model. **9**(3), 728–743 (2024)
13. Yagan, A., Jasmine, D.: Significance of an SEIHR model with preventive class in declining the spread of COVID-19. Indian J. Sci. Technol. **16**, 14–21 (2023)
14. Wang, J.J., Zhang, J.Z., Jin, Z.: Analysis of an SIR model with bilinear incidence rate. Nonlinear Anal., Real World Appl. **11**(4), 2390–2402 (2010)
15. Aybar, O.O.: Biochemical models of sir and sirs: effects of bilinear incidence rate on infection-free and endemic states. Chaos, Interdiscip. J. Nonlinear Sci. **33**(9), 093120 (2023)
16. Anggriani, N., et al.: Global stability for a susceptible-infectious epidemic model with fractional incidence rate. Appl. Math. Sci. **9**(76), 3775–3788 (2015)
17. Bentaleb, D., Amine, S.: Lyapunov function and global stability for a two-strain SEIR model with bilinear and non-monotone incidence. Int. J. Biomath. **12**(02), 1950021 (2019)
18. Sadki, M., Allali, K.: Stochastic two-strain epidemic model with bilinear and non-monotonic incidence rates. Eur. Phys. J. Plus **138**(10), 1–15 (2023)
19. Rajasekar, S., Pitchaimani, M., Zhu, Q.: Dynamic threshold probe of stochastic SIR model with saturated incidence rate and saturated treatment function. Phys. A, Stat. Mech. Appl. **535**, 122300 (2019)
20. Capasso, V.: Global solution for a diffusive nonlinear deterministic epidemic model. SIAM J. Appl. Math. **35**(2), 274–284 (1978)
21. Jan, R., Razak, N.N.A., Boulaaras, S., Rajagopal, K., Khan, Z., Almalki, Y.: Fractional perspective evaluation of Chikungunya infection with saturated incidence functions. Alex. Eng. J. **83**, 35–42 (2023)
22. Ilhem, G., Kouche, M., Ainseba, B.: Stability analysis of a fractional-order SEIR epidemic model with general incidence rate and time delay. Math. Methods Appl. Sci. **46**(9), 10947–10969 (2023)
23. Cui, X., Xue, D., Pan, F.: Dynamic analysis and optimal control for a fractional-order delayed SIR epidemic model with saturated treatment. Eur. Phys. J. Plus **137**(5), 1–18 (2022)
24. Din, A.: Bifurcation analysis of a delayed stochastic HBV epidemic model: cell-to-cell transmission. Chaos Solitons Fractals **181**, 114714 (2024)
25. Wang, N., Qi, L., Bessane, M., Hao, M.: Global Hopf bifurcation of a two-delay epidemic model with media coverage and asymptomatic infection. J. Differ. Equ. **369**, 1–40 (2023)
26. Zhu, L., Guan, G., Li, Y.: Nonlinear dynamical analysis and control strategies of a network-based SIS epidemic model with time delay. Appl. Math. Model. **70**, 512–531 (2019)
27. Barman, M., Mishra, N.: Hopf bifurcation analysis for a delayed nonlinear-SEIR epidemic model on networks. Chaos Solitons Fractals **178**, 114351 (2024)
28. Zhou, J., Zhao, Y., Ye, Y., Bao, Y.: Bifurcation analysis of a fractional-order simplicial sirs system induced by double delays. Int. J. Bifurc. Chaos **32**(05), 2250068 (2022)
29. Ashrafur Rahman, S., Zou, X.: Flu epidemics: a two-strain flu model with a single vaccination. J. Biol. Dyn. **5**(5), 376–390 (2011)
30. Khan, M.M.-U.-R., Arefin, M.R., Tanimoto, J.: Time delay of the appearance of a new strain can affect vaccination behavior and disease dynamics: an evolutionary explanation. Infect. Dis. Model. **8**(3), 656–671 (2023)
31. Diethelm, K., Ford, N.J.: Analysis of fractional differential equations. J. Math. Anal. Appl. **265**(2), 229–248 (2002)
32. Shah, K., Arfan, M., Ullah, A., Al-Mdallal, Q., Ansari, K.J., Abdeljawad, T.: Computational study on the dynamics of fractional order differential equations with applications. Chaos Solitons Fractals **157**, 111955 (2022)
33. Mainardi, F.: Fractional relaxation-oscillation and fractional diffusion-wave phenomena. Chaos Solitons Fractals **7**(9), 1461–1477 (1996)
34. Wu, Z., Cai, Y., Wang, Z., Wang, W.: Global stability of a fractional order sis epidemic model. J. Differ. Equ. **352**, 221–248 (2023)
35. Baleanu, D., Muslih, S.I., Rabei, E.M.: On fractional Euler–Lagrange and Hamilton equations and the fractional generalization of total time derivative. Nonlinear Dyn. **53**, 67–74 (2008)
36. Majee, S., Kar, T.K., Jana, S., Das, D.K., Nieto, J.: Complex dynamics and fractional-order optimal control of an epidemic model with saturated treatment and incidence. Int. J. Bifurc. Chaos **33**(16), 2350192 (2023)
37. Li, H.L., Zhang, L., Hu, C., Jiang, Y.L., Teng, Z.: Dynamical analysis of a fractional-order predator-prey model incorporating a prey refuge. J. Appl. Math. Comput. **54**, 435–449 (2017)

38. Li, Y., Chen, Y., Podlubny, I.: Stability of fractional-order nonlinear dynamic systems: Lyapunov direct method and generalized Mittag–Leffler stability. Comput. Math. Appl. **59**(5), 1810–1821 (2010)
39. Odibat, Z.M., Shawagfeh, N.T.: Generalized Taylor's formula. Appl. Math. Comput. **186**(1), 286–293 (2007)
40. Delavari, H., Baleanu, D., Sadati, J.: Stability analysis of Caputo fractional-order nonlinear systems revisited. Nonlinear Dyn. **67**, 2433–2439 (2012)
41. Cong, N., Tuan, H.: Existence, uniqueness, and exponential boundedness of global solutions to delay fractional differential equations. Mediterr. J. Math. **14**, 1–12 (2017)
42. Driessche, P., Watmough, J.: Reproduction numbers and sub-threshold endemic equilibria for compartmental models of disease transmission. Math. Biosci. **180**(1–2), 29–48 (2002)
43. Deng, W., Li, C., Lü, J.: Stability analysis of linear fractional differential system with multiple time delays. Nonlinear Dyn. **48**, 409–416 (2007)
44. Li, S., Bukhsh, I., Khan, I.U., Asjad, M.I., Eldin, S.M., Abd El-Rahman, M., Baleanu, D.: The impact of standard and nonstandard finite difference schemes on HIV nonlinear dynamical model. Chaos Solitons Fractals **173**, 113755 (2023)
45. Elbaz, I.M., Sohaly, M.A., El-Metwally, H.: Random dynamics of an SIV epidemic model. Commun. Nonlinear Sci. Numer. Simul. **131**, 107779 (2024)
46. Xiao, M., Jiang, G., Cao, J., Zheng, W.: Local bifurcation analysis of a delayed fractional-order dynamic model of dual congestion control algorithms. IEEE/CAA J. Autom. Sin. **4**(2), 361–369 (2016)
47. Cao, Y., Ren, W.: Distributed formation control for fractional-order systems: dynamic interaction and absolute/relative damping. Syst. Control Lett. **59**(3–4), 233–240 (2010)

Publisher's Note